2020-01-01

High Pressure High Heat Flux Pool Boiling Test Facility Design To Investigate Nucleation Boiling Heat Transfer Enhancement Using Micro/nano-Scale Engineered Structures

Omar Hernandez Hernandez Rodriguez
University of Texas at El Paso

HIGH PRESSURE HIGH HEAT FLUX POOL BOILING TEST FACILITY DESIGN TO INVESTIGATE NUCLEATION BOILING HEAT TRANSFER ENHANCEMENT USING MICRO/NANO-SCALE ENGINEERED STRUCTURES

OMAR HERNANDEZ RODRIGUEZ

Master's Program in Mechanical Engineering

APPROVED:

Md. Mahamudur Rahman, Ph.D., Chair

Jack F. Chessa, Ph.D.

Virgilio Gonzalez, Ph.D.

Stephen L. Crites, Jr., Ph.D.
Dean of the Graduate School

Dedication

I dedicate this writing to my parents, brothers, and to my love for all their support along my studies.

HIGH PRESSURE HIGH HEAT FLUX POOL BOILING TEST FACILITY DESIGN TO INVESTIGATE NUCLEATIOATE BOILING HEAT TRANSFER ENHANCEMENT USING MICRO/NANO-SCALE ENGINEERED STRUCTURE

by

OMAR HERNANDEZ RODRIGUEZ, M.S.

THESIS

Presented to the Faculty of the Graduate School of

The University of Texas at El Paso

in Partial Fulfillment

of the Requirements

for the Degree of

MASTER OF SCIENCE

Department of Mechanical Engineering

THE UNIVERSITY OF TEXAS AT EL PASO

August 2020

Acknowledgements

The work described in this thesis would not have been possible without the direct participation of my mentor Dr. Md. Mahamudur Rahman.

I thank the Mechanical Engineering Department of UTEP for supporting me with a teaching assistantship, and I thank the cSETR for all the support given in this last year. I also thank Angel Lerma and Arturo Reyes from the UTEP machine shop for all the support and guidance for machining this pool boiling facility.

Finally, I also thank the members of my thesis committee, Dr. Jack F. Chessa and Dr. Virgilio Gonazalez, for their careful reading of this thesis, and all of my professors and the staff of the Mechanical Department for their continuous support during these two years.

Abstract

Developing efficient heat dissipation technologies is of critical importance towards the development and the commercialization of next-generation compact and high-performance electronic devices, cooling systems, power generation systems and chemical processing units, as well as retrofitting the existing thermal management schemes. As such, phase change heat transfer systems, more specifically boiling heat transfer systems, have attracted significant attention due to their ability to extract a large amount of latent energy stored within the fluid. Pool boiling is an efficient mode of phase change heat transfer processes accompanied by nucleation of vapor bubbles from liquid on to the hot surfaces, bubble growth, and departure from the heated surface in a stagnant liquid. Noticeably, boiling becomes vigorous and more effective at higher power as vapor production increases with increasing the surface temperature. However, if the applied power from the industrial systems exceeds the upper governing limit of a heat transfer surface, which is also termed as the critical heat flux (CHF) limit, a drastic increase in surface temperature occurs leading to system failure. This occurs due to the formation of a stable vapor film on the heated surface that creates insulation effect in between the hot surface and coolant. It is therefore essential to design and develop advanced thermal management schemes to further increase the surface maximum heat transfer capability (CHF) limit.

Motivated by these goals, in the last decades, several researchers have explored solutions to enhance the limits of boiling heat transfer. By manipulating the solid-liquid-vapor interface using these structures, more than 100% increase in boiling heat transfer has been realized. The reasons of this significant enhancement are typically attributed to the surface roughness, wettability, and capillary wicking. Several engineered surfaces have been considered, including hydrophilic porous layers, nanowires, nanorods, oxide nanostructures, micropillars, hoodoos, micro-ridges, hierarchical structures and many others. However, this massive heat transfer enhancement has only been demonstrated on flat surfaces, whereas, in reality, vast majorities of industrial heat transfer surfaces are of tubular geometries. Additionally, the boiling mechanism is

significantly different between flat surface and tubular surface. For instance, different from flat surface, local heat transfer on a tubular surface is primarily governed by the liquid convection in the bubble layer around the tube and evaporation under the sliding bubbles. Thus, it is important to experimentally demonstrate the heat transfer enhancement on these curved surfaces utilizing the advanced micro/nano-structures for the industrial applications. Moreover, these reported enhancements are limited to atmospheric pressure boiling conditions as opposed to the high-pressure environment in industrial applications. Additionally, several CHF correlations for engineered surfaces have been reported by the scientists in the last one decade; still, there is no general agreement on the enhancement mechanisms. Again, these models were developed for the planar surfaces at atmospheric boiling conditions. In this regard, this thesis aims to design and develop a high-pressure high heat flux pool boiling test facility for micro/nano-engineered rods using water as the working fluid and capable of operating up to 20 bar pressure.

Table of Contents

List of Tables

List of Figures

Chapter 1: Introduction

1.1 Phase Change

Phase change heat transfer is used in a vast number of applications and is critical for large-scale industrial processes as well as small-scale thermal management systems. As such, even modest enhancements in phase change heat transfer efficiency can lead to substantial energy and cost savings.

Some important applications are power generation, distillation, chemical processing, cooling of nuclear reactors, HVAC application, heat pipe/ electronic cooling, etc. Phase change heat transfer is present in pool boiling, flow boiling, spray cooling, condensation.

1.2 Pool Boiling

Pool of motionless with any liquid with a type of surface getting heat and facing boiling on its surfaces is generally referred as pool boiling. Pool boiling heat transfer is the process of vigorous heat transfer occurring with a phase change from liquid to vapor. Numerous researchers started looking into boiling phenomenon since Nukiyama [1] where he conducted a pool boiling experiment with the analyses base in experimental data plotted of the wall super heater temperature versus the heat flux.

The boiling heat transfer has received considerable attention due to the effort coming from modern developments in technology [2]. The necessity to remove large amounts of heat from hot bodies guide researchers to investigate and understand boiling heat transfer [3]. Pool boiling has several applications in electronics, pressurized water reactors (PWR), space applications. Therefore, there are several reports in literature about pool boiling on flat engineering surfaces reporting CHF enhancements with different surface roughness [4], with nanofluids [5], microchannels [6], etc. The enhancement of CHF and Heat transfer coefficient (HTC) are very important to develop new technologies that can fulfill the high requirements in complex

applications. These new applications require more complex shapes capable to remove heat from them. For this reason, researchers such as Kandlikar, Kulenovic et al. [7], Kim and Choi [8], and more started to investigate on pool boiling on cylindrical engineering surfaces. Consequently, this thesis presents a complete design of a pool boiling facility to test cylindrical engineering surfaces at high heat flux and high pressure to contribute to the understanding of the physics behind this phenomenon that can improve several applications in the future.

The regimes of pool boiling are easily understood in terms of the so-called boiling curve where these parameters are plotted with values called heat flux q'' versus superheated wall temperature minus saturation temperature ($T_w - T_{sat}$). The pool boiling curve were determined for the first investigations performed by Nukiyama[1], Jakob and Linke [9], and Drew and Muller [10]. Pool boiling curve applied to well-wetted surfaces for which the characteristic physical dimension L is large compared to the bubble or capillary length scale L_b defined as [11]

$$L_b = \sqrt{\frac{\sigma}{g(\rho_l - \rho_v)}} \tag{1.1}$$

The pool boiling regimens can be observed in Figure 1.1 and Figure 1.2. If the value of the excess temperature increases, the curve faces 5 different regimes:

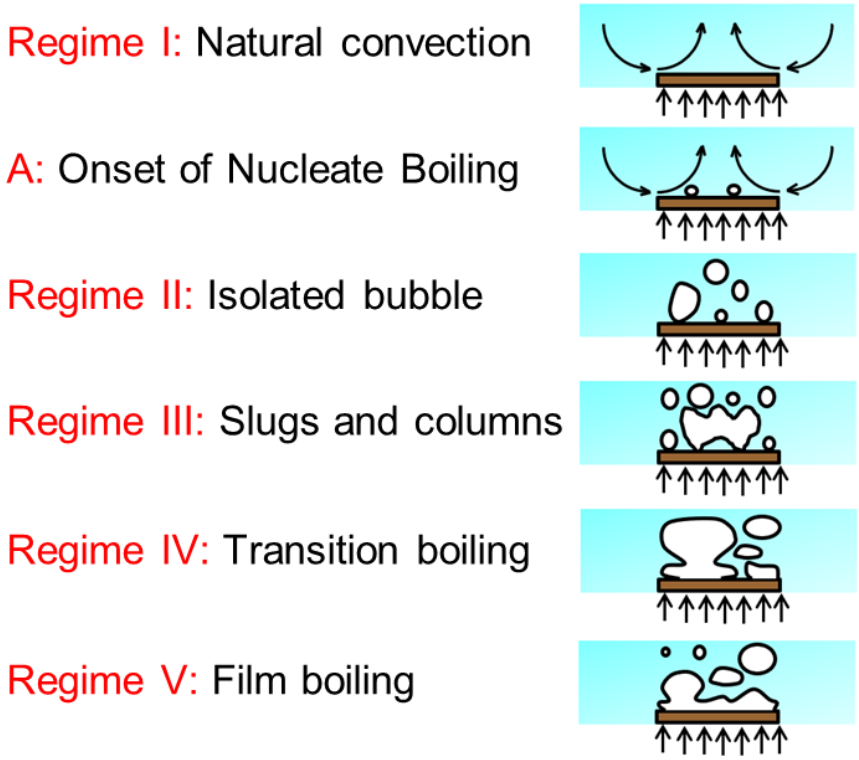

Figure 1.1: Typical Pool Boiling Bubble Regimes. [12]..

- Region I, Natural Convection.

Represent natural convection boiling where no bubbles are forming on the heating surface. Bubbles will start forming after point A, this is the onset of nucleate boiling.

- Region II, Isolate bubble

Nucleation boiling is represented in the region II where the first bubbles start forming in preferential sites on the heating surface due to vapor trapped on the surface or non-condensable gases. Fully developed nucleation boiling will be formed in point B.

- Region III, Slugs and columns

Slugs and columns of bubbles are visible. The film boiling is not present and bubbles columns are perfectly defined. The critical heat flux (CHF) is reached in point C.

- Region IV, Transition Boiling.

Nucleate and film boiling partially occur together. Closer to point D called minimum heat flux point, the film boiling is getting more visible.

- Region V, Film Boiling.

After point D, the heater surface is completely covered by a continuous stable vapor film and the surface will fail at pint E.

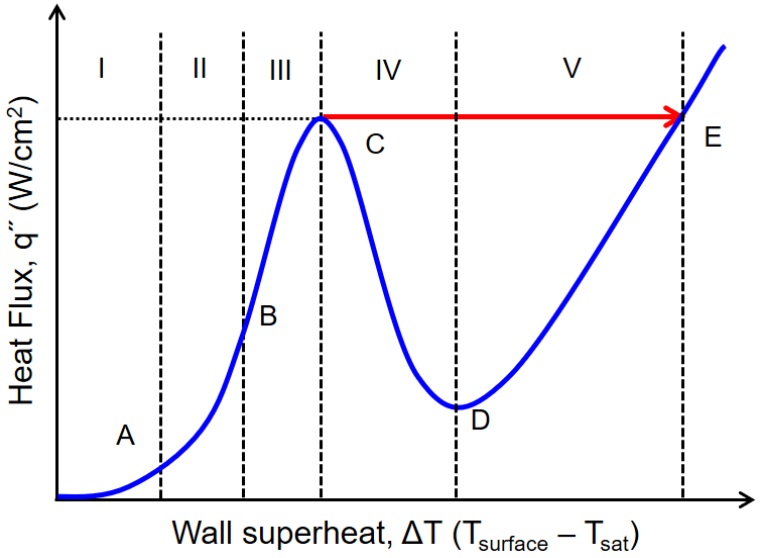

Figure 1.2: Typical Water Boiling Regimes Graph Curve at one Atmosphere. [12].

1.3 Critical Heat Flux (CHF)

Dissipation of heat from any surface has a finite rate called critical heat flux (CHF). Critical heat flux is a finite rate of extraction of heat from any surface. During Boiling, there is a process where heat transfer is control by some step such as waiting period, nucleation, bubble growth, and

bubble departure from a surface. This process removed large amounts of heat from the surfaces due to the phase change. When a phase change occurs during heating a surface with any working fluid CHF describes the thermal limit of the tested surface. CHF limits the use of boiling in all the industrial applications. For example, the more important problem in industries is the boiling limitation that it is directly related to the burnout of the materials of a heated surface due to the combination of bubbles creating a vapor film that decreases the heat transfer on the surface to the liquid. Due to this vapor film the temperature on the material increases and fails. Due to this failure on many applications for heat removal from surfaces, many researchers are working on increase the CHF because is the principal limitation on designs and operations condition for boiling systems.

1.4 HEAT TRANSFER COEFFICIENT (HTC)

CHF is responsible of define the values of operations on any boiling system. However, heat transfer coefficient (HTC) define the efficiency of boiling. HTC is used to calculate the heat transfer. There are two typically cases for HCT such as convection or phase change between a fluid and a solid, it is defined as the ratio of surface heat flux or thermal power per unit area to the superheat temperature that refers to the difference of temperature between the solid surface and surrounding saturation temperature of the fluid as given by Eq. (1.2).

$$HTC = \frac{q''}{\Delta T} \tag{1.2}$$

Chapter 2: Literature Review

2.1 Boiling on Planar Surfaces

2.1.1 Bubble Nucleation

Heterogeneous nucleation is present in many applications, heat is transferring through a solid wall that contains the liquid. The wall transfers enough heat to the nearest water and this water may reach and slightly exceed the equilibrium saturation temperature; this is called thermal boundary layer. The embryo is formed at the solid interface because the highest temperature is there due to the convection heat transfer. The bubble will nucleate if there is a cavity in the heated surface with some vapor non-condensable gas trapped in this cavity. In general, the contact angle and interface tension will dictate the vapor embryo shape at the surface of a flat surface, the profile shape of the vapor embryo in a flat and hydrophobic surface in a conical cavity is shown in Fig.2.1.

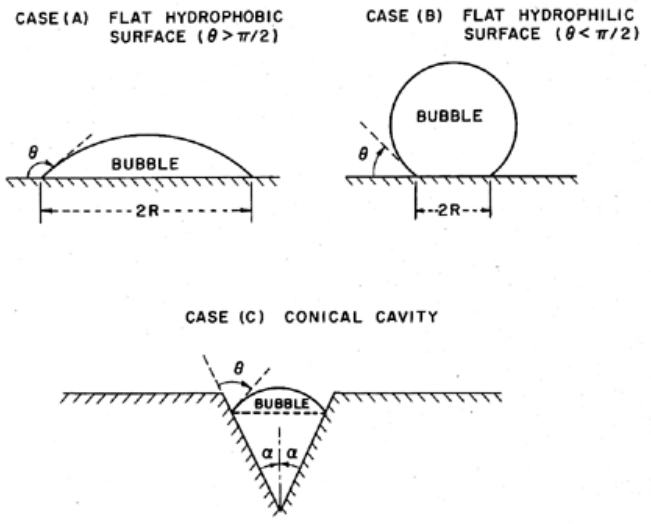

Figure 2.1: (A) Flat hydrophobic surface. (B) Flat Hydrophilic cavity surface. (c) Conical cavity.[13]

2.1.2 Criteria for A Bubble to Grow from A Cavity

Hsu criterion [14] describes the criteria for a bubble to grow from a cavity where this criterion predicts two important features of the heterogeneous nucleation on a heated wall. The first point explained is that before any active nucleation site appears, a minimum value of wall super-heated should be attained. The second point stated that a finite number of active nucleation sites will be present with a temperature above the superheat required. The extend of these active range of cavities depend on the fluid properties, δ_t, and the subcooling of the bulk fluid. Hsu found that its correlations predict and are consistent with the values obtained from experimental observations by Clark et al. [15]. The following equation predicts the range of active cavity sizes by Hsu correlation:

$$\begin{Bmatrix} r_{c,min} \\ r_{c,max} \end{Bmatrix} = \frac{\delta_t}{4}\left[1 - \frac{\theta_{sat}}{\theta_w}\begin{Bmatrix} + \\ - \end{Bmatrix}\sqrt{\left(1 - \frac{\theta_{sat}}{\theta_w}\right)^2 - \frac{12.08\sigma T_{sat}(P_l)}{\rho_v h_{lv}\delta_t \theta_w}}\right] \tag{2.1}$$

where $r_{c,min}$, $r_{c,max}$, δ_t, θ_{sat}, θ_w, σ, $T_{sat,}$ T_w, ρ_v, h_{lv} are minimum cavity mount radius, maximum cavity mount radius, thermal boundary layer thickness, $\theta_{sat} = T_{sat} - T_\infty$, $\theta_w = T_w - T_\infty$, interface tension, saturation temperature, wall temperature, vapor density and latent heat of vaporization per unit mass, respectively. In Fig. 2.2, it can be observed a range prediction of active cavity sizes using Hsu's analysis. In Fig. 2.3, it can be observed the system considered in Hsu's model.

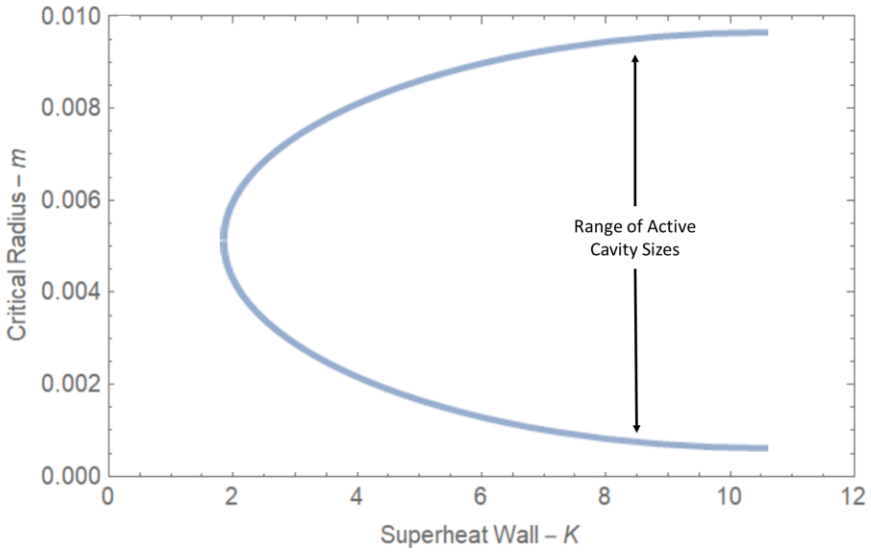

Figure 2.2: Range Prediction of Active Cavity Sizes Using Hsu's Analysis.[16].

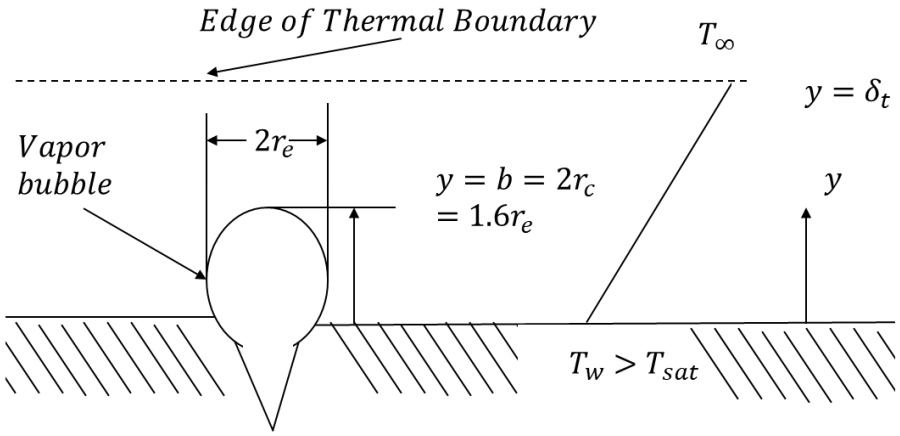

Figure 2.3: Model ebullition cycle.[16].

It is known that the criteria for a bubble to grow from a cavity with vapor trapped is describe by the Hsu criterion Eq. 2.1. Now, the equation that quantifies this phenomenon is the Young-Laplace equation:

$$p_g - p_f = \frac{2\sigma}{r^*} \tag{2.2}$$

where p_g, p_f and r^* are the gas pressure, fluid pressure and the critical radius of the bubble, respectively. The bubble growth can be considered as an idealized process consisting in a sequence of stages as it is shown in Fig. 2.4. The first step (a) of this idealized process is the waiting period that corresponds to the period after the bubble departure to the instant when a new bubble is nucleated at the nucleation site. The second step (b) corresponds to the beginning of the bubble formation. The third step (c) describes a bubble growth due to a vapor generation via microlayer evaporation. The fourth step (d) describes a bubble growth due to the dry spot under the bubble. The fifth step (e) the bubble growth is getting a large diameter, the buoyancy force is greater and the contact surface of the bubble with the heated surface is decreasing and now, a contact ring is visible. Finally, (f) describe the time required from Waiting period to the bubble departure from the heated surface.

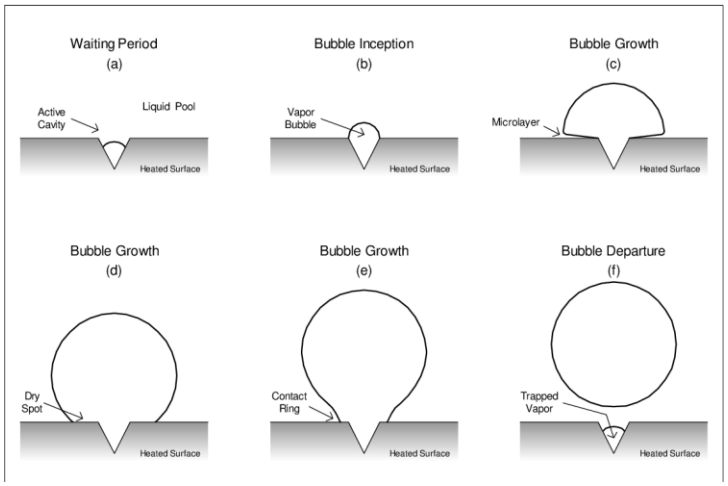

Figure 2.4: Bubble Grow as Idealized Process [17].

2.1.3 Departure Diameter and Release Frequency of a Bubble

The ebullition cycle is a complete set of steps such as liquid heating, nucleation, bubble growth and release. Bubble diameter at departure,d_d, and frequency, f, directly affect the rate of heat transfer during the process of extraction of heat from a heated surface. These two factors were related for previous researchers [9,10].

There is a direct relation between d_d and departure Bond number,Bo_d, defined as

$$Bo_d = \frac{g(\rho_l - \rho_v){d_d}^2}{\sigma} \tag{2.3}$$

where Bo_d is a dimensionless number.

There are many attempts of correlations that described this phenomenon. Peebles and Garber [20] proposed the relation

$$f d_d = 1.18\left(\frac{t_g}{t_g + t_w}\right)\left[\frac{\sigma g(\rho_l - \rho_v)}{{\rho_l}^2}\right]^{\frac{1}{4}} \tag{2.4}$$

where t_w is the waiting time and g is the growth time to the departure diameter. There are more equations that describe this phenomenon but more experimentation is required to find a correlation that accurately describes and related bubble growth and release.

2.2 Boiling on Curve Surfaces

Boiling in curve surfaces has a large amount of applications in real life. Nowadays, researchers investigate boiling on curve surfaces. Almost all the industrial applications use tubes to transport liquids, one example of this applications can be a power water reactor PWR where the flowing water touch the nuclear rods created a boiling on their surface. Other important application is the refrigerant flowing inside the tubes of the radiator of a car, this refrigerant is cooling down

the car's motor. there is a large demand for part of the industry at the science community to look for curve surfaces capable to increase the CHF and HTC to reduces cost and increase efficiency. Due to the necessity on industries many researchers have been testing on planar surfaces but a small quantity of teams has been testing on cylindrical surfaces.

2.3 BOILING ENHANCEMENT

Nowadays, humans are looking for the development of more compact cooling devices capable of increased the HCT and CHF, saving a huge amount of energy and cost in this type of heat transfer applications. It is reported in literature that increasing the CHF will result in a direct increased in power density in pressurized water reactors, giving a positive impact in the cost for electrical generation [21]. It is well known that pool boiling is affected directly by the fluid properties, pressure, surface properties such as roughness, hydrophobic surfaces, hydrophilic surfaces, power of the heater and orientation.

2.3.1 Boiling Enhancement by Changing Fluid Properties

There are several popular working fluids in pool boiling such as water, Isopropyl alcohol, Freon 11, FC-72, FC-87, R113, etc. Each liquid has its own thermal properties, for that reason the boiling curve is different for each one. A simple way to increase performance on pool boiling is the effect of pressure [22]. Another method widely used is enhancing the thermal properties of the fluid such as micro/nano scale thermally conductive particles into the boiling fluid such as A_2O_3, silica, TiO_2,carbon nanotubes, etc. [24-27].These are two ways to improve the pool boiling performance and increase values of CHF and HTC. In Fig.2.5. It can be observed boiling behaviors at different heat fluxes [23].

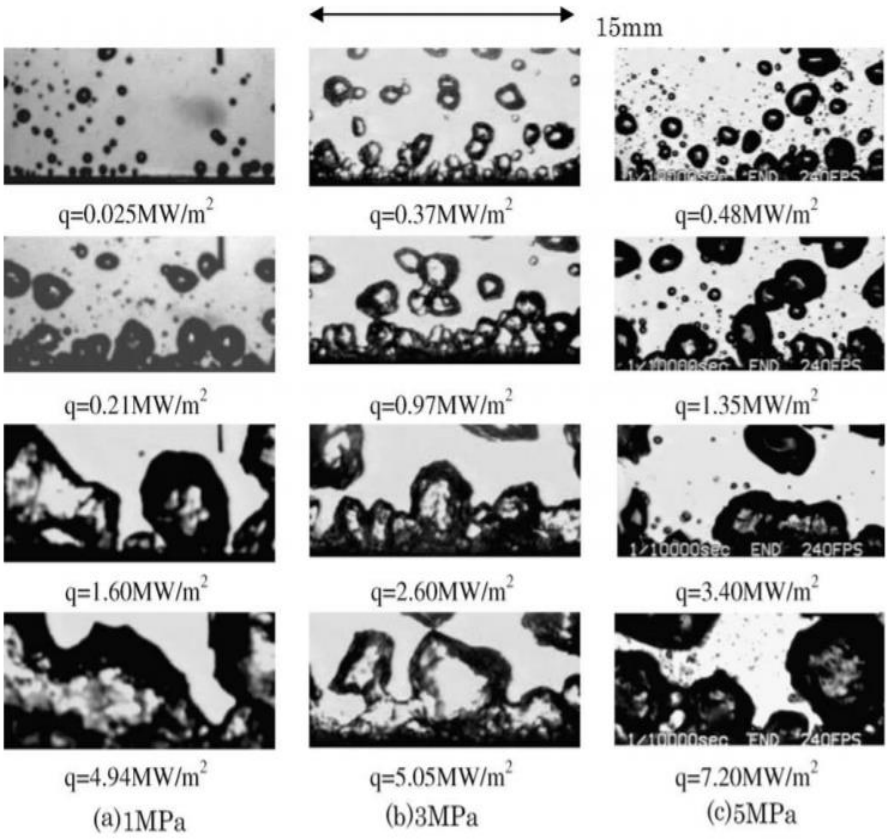

Figure 2.5: Boiling Behaviors a Different Heat Fluxes and Different Pressures [23].

2.3.2 Boiling Enhancement on Planar Surfaces

Enhanced surfaces play a very important role in boiling heat transfer. Some examples of engineering surfaces are micro/nano structures in the surfaces, deposition coatings to create hydrophobic and hydrophilic surfaces where these coats can change the wettability. The boiling performance can be increase due to the heat transfer area. If there is more transfer area for boiling, it is possible to have more vapor or non-condensable gases on the surface capable of increasing the nucleation site's density, bubble sizes frequencies and capillary wickability. There are two main factors to improve boiling on a surface, the first is the structured surfaces and the second one is the surface wettability. Structure surfaces are modifications on the top of a surface creating

roughness, this roughness is a very powerful tool to enhance the performance of pool boiling because it creates favorable conditions for bubble nucleation.

K. Takata et al [24]. show research on superhydrophylic surfaces with a CHF enhancement closed to 200 percent, see Fig. 2.6. On the other hand, McHale and Garimella [25] presented a study in smooth and rough surfaces with an enhancement from 15 W/cm² to 19 W/cm² approximately, see Fig. 2.7.

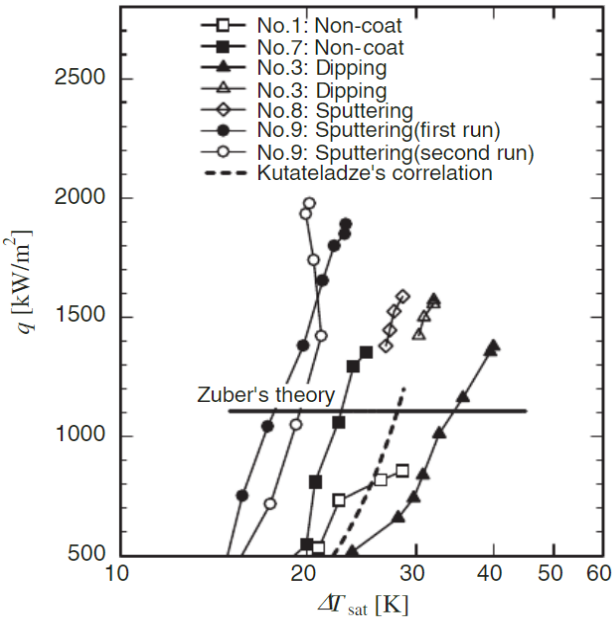

Figure 2.6: Boiling Curves for superhydrophilic surfaces [24].

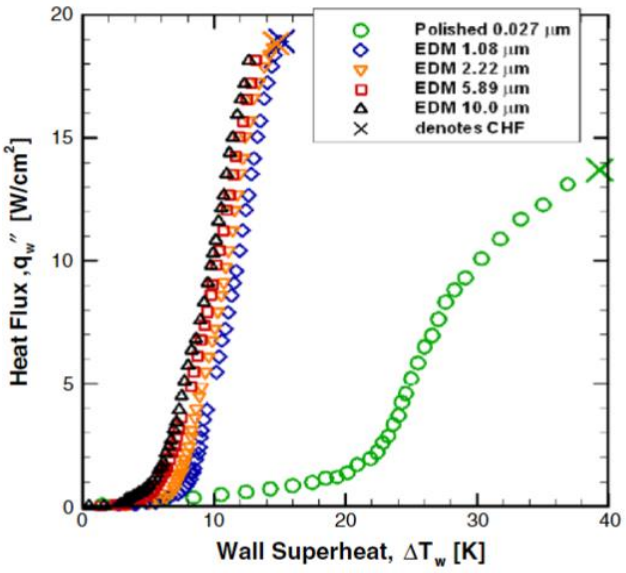

Figure 2.7: Boiling Curves for FC-77 on five surfaces of varying roughness [25].

Launay et al [26] investigated in a hybrid micro-nano structure thermal interfaces for pool boiling. In Fig.2.8 is observed a sample fully coated with carbon nanotubes (a), in (b) it is shown silicon pin-fins structure, and finally, carbon nanotube pin-fin array (c). Launay et al. presented enhancement for 3D structures with a CHF of 24 W/cm².

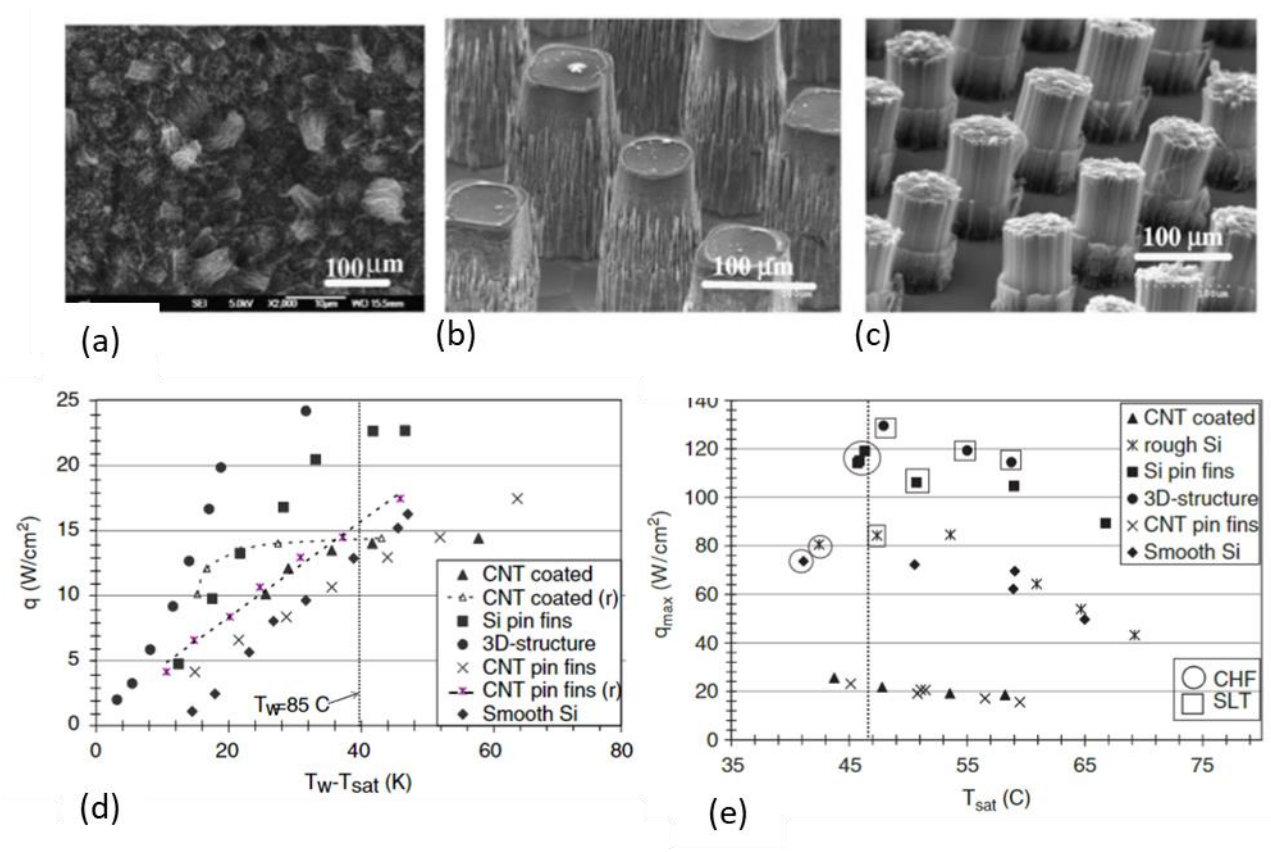

Figure 2.8: (a) SEM showing a top view of the sample fully coated with carbon nanotubes. (b) SEM of the silicon pin-fins structure. (c) SEM of the carbon nanotube pin-fin array, (d) Boiling Curve for PF5060 with Coated Nano Tubes (CNT), (e) Boiling Curve for Water with different Enhance Structures.[26].

There are several methods to create roughness such as chemical etching [25-27], sanding [28-29], micropins [30-31], etc. The availability today of microfabrication and surface techniques allows for many advanced modifications to be made to the surface of the materials to be tested. The enhancement of these techniques allows for the fabrication of structures and surfaces such as micro-pillared surfaces [32-34], micro channeled surfaces [35-37], nano porous surfaces [38-40], hierarchically structured surfaces [41-43], etc. The performance on boiling can be directly affected on these micro/nano structures by shape, length, and configurations of these geometries. Previous research has shown that CHF and HTC are increased by the microstructure surfaces [44-46].

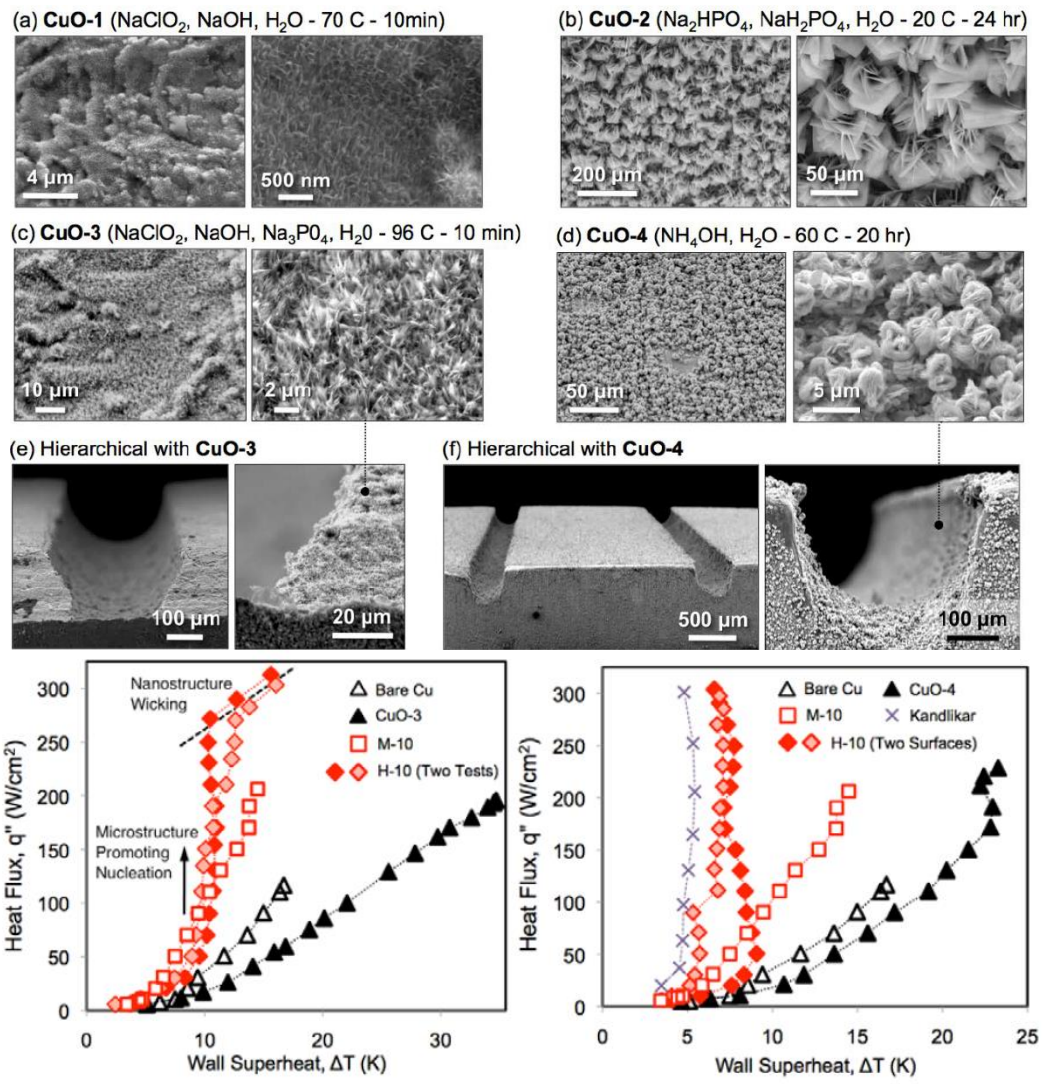

Figure 2.9: Pool boiling heat transfer enhancement using engineered micro/nano hierarchical channel surfaces: (a) – (d): fabricated four different nanostructures, (e) - (f): nanostructures on micro-channel surfaces [49].

Several researchers have been reporting enhancements on the limits of the boiling heat transfer specially in advanced fabrication technologies such as micro-and nano-scale features to the boiling surfaces. It can be highlighted that other research exists on engineered surfaces for techniques already mentioned with additive features as well as subtractive features such as hydrophilic porous layers[50], nanowires[52-53], nanorods[54], oxide nanostructures [43], micropillars [51], hoodoos[52], micro-ridges [55, 56], and hierarchical structures [57-58]. As of today, these surfaces have been shown to increase the pool boiling CHF ranging from +30% to +240% as compared to

the reference heaters. A representative pool boiling heat transfer enhancement using surfaces engineering has been shown in Fig. 2.9, reported by Rahman et al [49]. Four different nanostructures and five different microchannel structures were incorporated in flat copper surfaces, and significant CHF and HTC enhancement has been demonstrated.

2.3.3 Boiling Enhancement on Cylindrical Surfaces

Researchers has been studying nucleation heat transfer and they have identified different techniques for increase CHF and HTC. This techniques can be classified into four categories: re-en-trant cavities, porous surfaces, surface roughness and tube orientation, and microchannels/integral fins [6]. Mehta and Kandlikar presented an enhancement method of circumferential rectangular open microchannels where they vary the fin width, channel width, deep and pitch, see Fig. 2.10. They found an increase on CHF almost of 200% compared with a cylindrical sample without any modification on the surface.

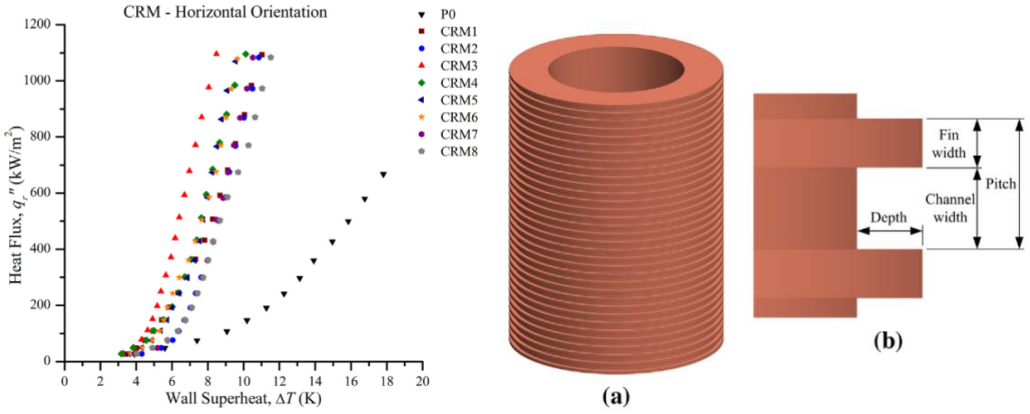

Figure 2.10: Boiling curves for the CRM test sections in the horizontal orientation,(a) CRM test section, (b) key geometric parameters required to defined a CRM test section.[6].

On the other hand, Kuman et al.[60], they presented a heat transfer enhancement on cylindrical surfaces with hybrod wettable patters, see Fig.2.11. They make coatings on the surfaces of cylindrical surface with superhtdrophilic SiO_2.

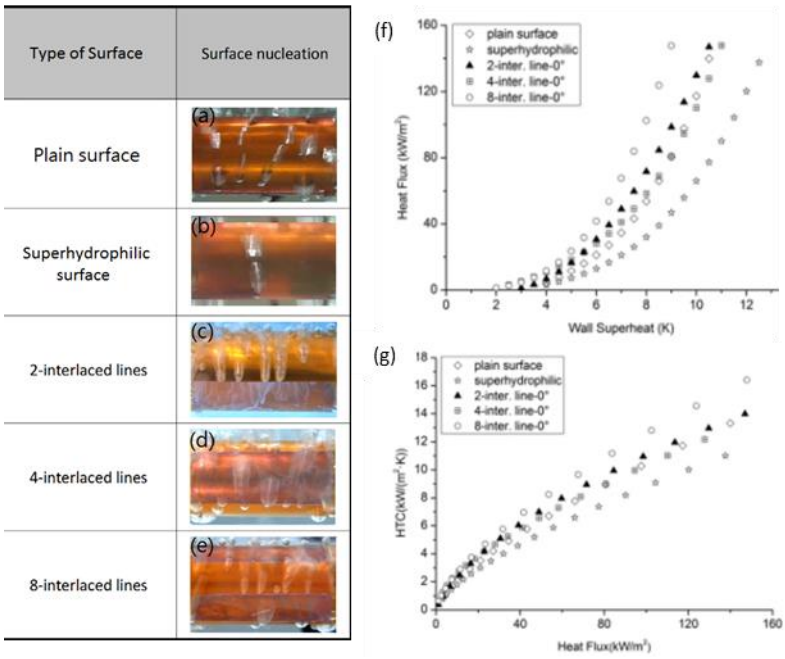

Figure 2.11: Photographs of bubble nucleation. (a) Plain surface. (b) Superhydrophilic surface. (c) 2-interlined surface. (d) 4-interlined surface. (e) 8-interlined surface. (f) Boiling curves for the various surfaces. (g) Graph of the HTC versus the heat flux. [60].

Kumar et al., in (2017) tested samples with wettable structures on cylindrical copper surfaces. They tested plain surface, superhydrophilic surfaces, printing the polymethyl methacrylate (PMMA) polymer, hydrophobic patterns, superhydrophilic and hydrophobic patterns, see Fig. 2.12. where the combination of superhydrophilic and hydrophobic patterns shown a good enhancement on the creation and control of new nucleation points[61].

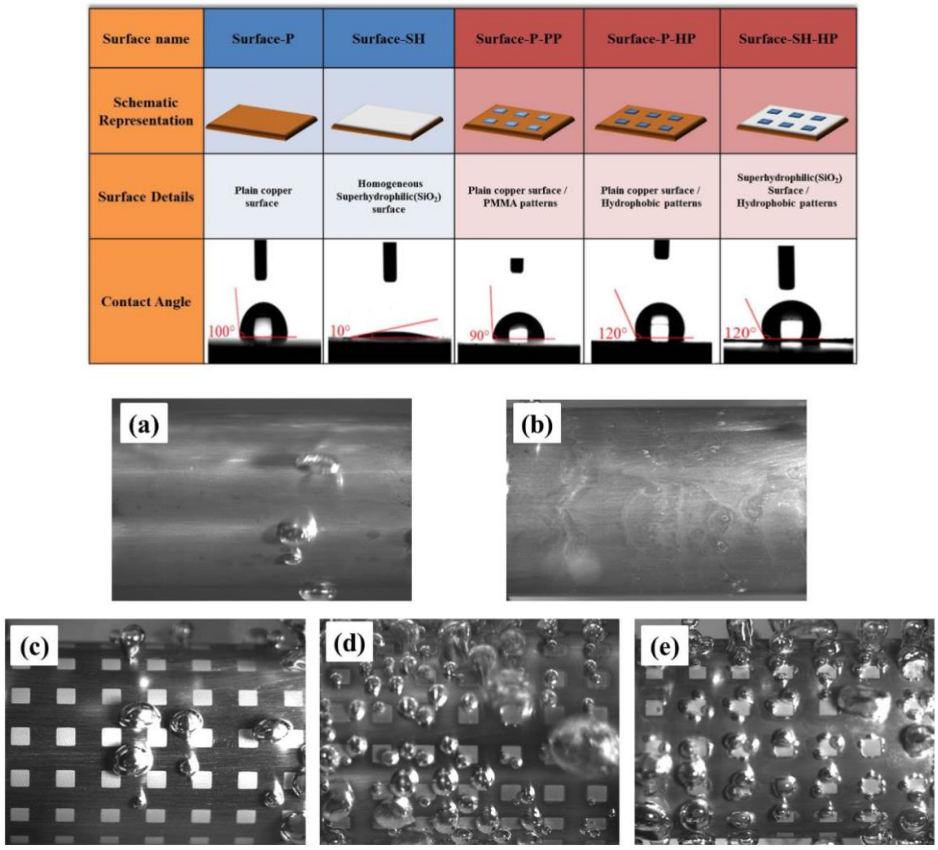

Figure 2.12: Schematic representation of different surfaces and its details and contact angles. Comparison of bubble formation density of different tested surfaces at 30 W power input (a) Surface-P, (b) Surface-SH, (c) Surface-P-PP, (d) Surface-P-HP, and(e) Surface-SH-HP. [61].

2.4 Critical Heat Flux Models

2.4.1 Critical Heat Flux Models on Planar Surfaces

The few last decades, researcher has been looking for a universal model capable to describe the CHF in pool boiling, many researchers have developed models that describe the behavior of CHF but no one has developed a correlation that can join all the parameter in a simple equation.

In 2001, Kandlikar [62] developed a theoretical model to predict pool boiling CHF incorporating effects of contact angle and orientation where he developed a correlation for critical heat flux and a kandlikar constant “k”.

$$q''_{CHF} = k\,\rho_v^{1/2} h_{lv} [\sigma(\rho_l - \rho_v)g]^{1/4} \quad (2.5)$$

$$k = \frac{1+\cos\theta}{16}\left[\frac{2}{\pi}+\frac{\pi}{4}(1+\cos\theta)\cos\varphi\right] \quad (2.6)$$

2.4.2 Critical Heat Flux Models on Engineering Surfaces

Chu et al. proposed a correlation for surface roughness augmented wettability on CHF during pool boiling. This correlation describes the enhancement on CHF on roughness surfaces, the equation is based on Eq. 2.5 using a new constant "k"

$$k = \frac{1+\cos\theta}{16}\left[\frac{2(1+\boldsymbol{r}\cos\theta)}{\pi\,(1+\cos\theta)}+\frac{\pi}{4}(1+\cos\theta)\cos\varphi\right] \quad (2.7)$$

Rahman et al.[63], presented a study for predicts the CHF bare surfaces based on surface contact angle. It was demonstrated that their results coincide with the Kandlikar model pool boiling CHF model but this Kandlikar model cannot predict CHF for enhanced surfaces. Rahman et al. presented a correlation using a dimensionless wicking number, Wi, where is given by

$$Wi \equiv \frac{\dot{V_0}''\rho_l}{\rho_v^{1/2}[\sigma(\rho_l-\rho_v)g]^{1/4}}k \quad (2.8)$$

where Wi is the nondimensional form of the wicked volume flux and $\dot{V_0}''$ will dictate CHF enhancement.

On the other hand, Dhillon et al., They demonstrated the existence of maxima in CHF enhancement at the texture density. This model is based on characteristic dry spot heating and re-wetting time scale represented by

$$q''_{CHF,W} = \rho_s C_s t_s (T_{crit} - T_0)\times\left[\left(\frac{4\Delta\rho g^3}{\sigma}\right)^{1/4}(1-\tau_r)+\max\left(0,\frac{2\Delta\rho g K_v P_c}{\mu\sigma}\right)\right] \quad (2.9)$$

2.5 BOILING TEST FACILITIES

2.5.1 Boiling Test Facilities on Planar Surfaces

Pool boiling research faces two main problems. The first one, and not so difficult to defeat is the high-pressure design for a chamber capable of withstanding temperatures around 340 ˚C or even higher. The second one, is the design of the main heater capable to reach high heat fluxes up to 10 MW/m² over cylindrical tubes. There is much research on pool boiling flat surfaces with different engineering structures or nano/fluids but with low pressure and low heat fluxes due to the availability of heaters with a low power capability.

Buongiorno *et al.* present results for pool boiling facility working from 0.02- 2 bar with a maximum critical heat flux as high as 6MW/m² for flat surfaces with nanofluids with this type of configuration. The MIT nanofluid pool boiling facility can be observed in Fig. 2.13 where an ITO glass heater is located[64].

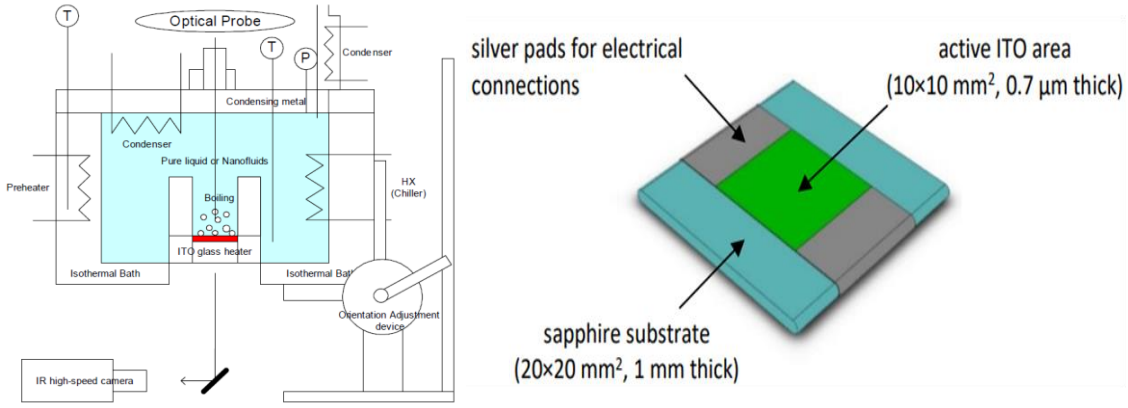

Figure 2.13: MIT nanofluid pool boiling facility and heater [64].

Rahman [12] presented a pool boiling experimental setup used for testing saturate water, see Fig.2.14.. This facility uses a copper block with two cartridge heaters embedded in to the copper block allowing a maximum power of 1000. The test facility was used at atmospheric pressure but it can test other fluids and it can hold high pressure at low CHF.

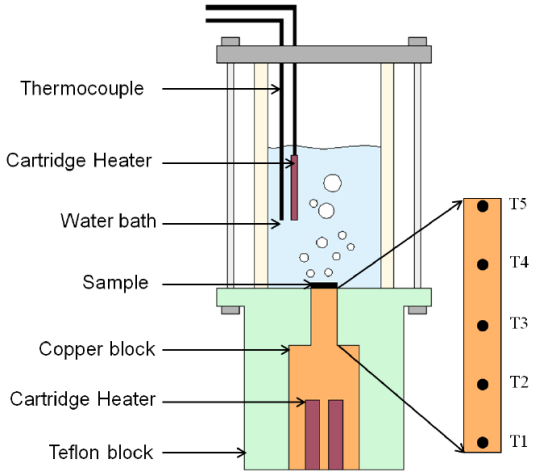

Figure 2.14: Schematic of pool boiling experimental setup for water.[12].

Jaikumar and Kandlikar [38] presented a pool boiling facility with tests of water at atmospheric pressure, see Fig.2.15. The maximum CHF of 313 W/cm² with a sintered-throughout surface with 2.4 fold enhancement in CHF over a plain chip.

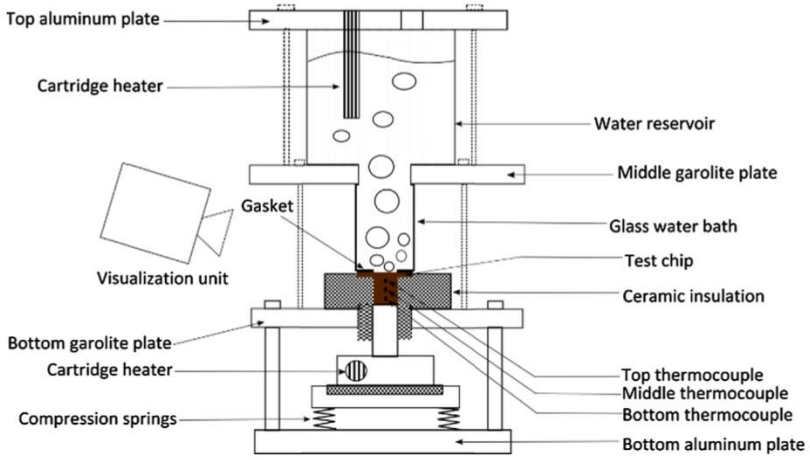

Figure 2.15: Schematic of pool boiling experimental for chip tests. [38].

2.5.2 Boiling Test Facilities on Cylindrical Surfaces

For example, Mehta and Kandlikar performed experiments over cylindrical tubes with water at atmospheric pressure using microchannels over the tested cylindrical sample. In Fig. 2.16(a), it can be observed a CAD model of the experimental setup used for Mehta and Kandlikar where it can be seen a test section assembly, auxiliary heater, silicon gaskets and compression plates.

The Test section assembly is shown in Fig. 2.16(b), the tested sample is placed on the main heater with a gasket and ceramic insulation on both sizes. Finally, the sample with the gaskets and insulations are compressed by 4 screws in a cylindrical pattern shape. The maximum heat flux reported is up to 1.1 MW/m². In this case, there is high heat flux but at atmospheric pressure.

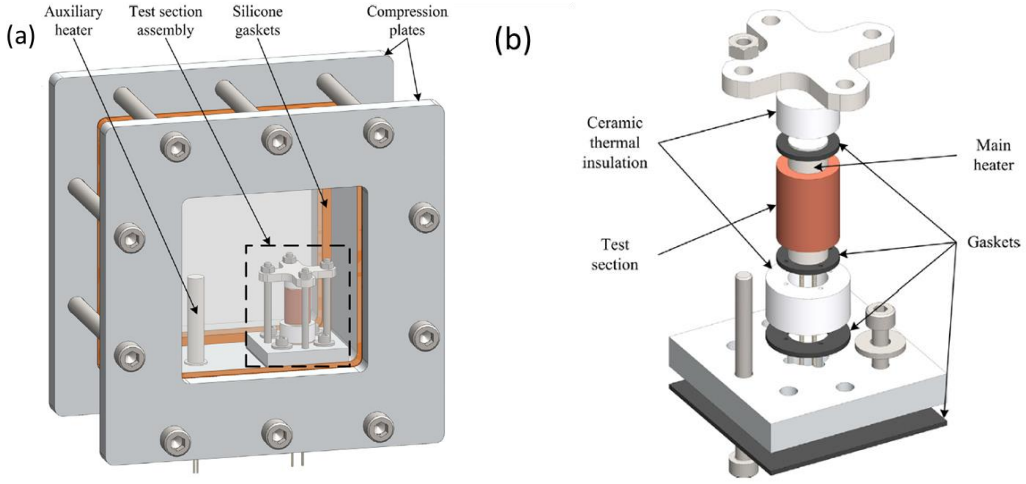

Figure 2.16: (a) Experimental setup for pool boiling, (b) Exploded view of the test section assembly [64].

On the other hand, Kulenovic et al. have a test facility that can work a pressure up to 16 bar but, they performed experiments with heat fluxes below 10 kW/m² [7]. A cartridge heater with a power of 950 W was used due to the unavailability in the industry of this small heater with high power capacity, the design of the sample heater is a huge challenge. In Fig. 2.17, the schematic setup for the heater and cylindrical sample can be observed.

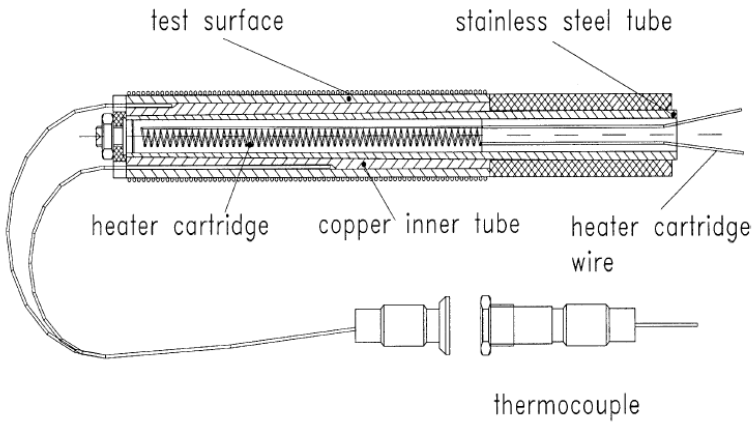

Figure 2.17: Schematic arrangement of the test specimen for structured tubular heat transfer surfaces [7].

Kim and Choi investigated on structured tubes with pores, they tested up to 40 kW/m² at a saturation temperature of 4.4 ˚C. for different refrigerants such as R-11, R-123 and R-134a [8]. In Fig. 2.18(a), the schematic drawing of the experimental setup can be observed. In Fig. 2.18(b). a sketch of the test tube configuration used in this experimentation is observed.

From Table 2.1, it can be observed the research on cylindrical engineering surfaces tested on pool boiling, almost all the researche is performed atmospheric pressure due to the difficulty of designing a heater capable to reach high heat fluxes [64]. For that reason, this thesis is focused on the design of a pool boiling facility over cylindrical engineering surfaces at high pressure high heat flux.

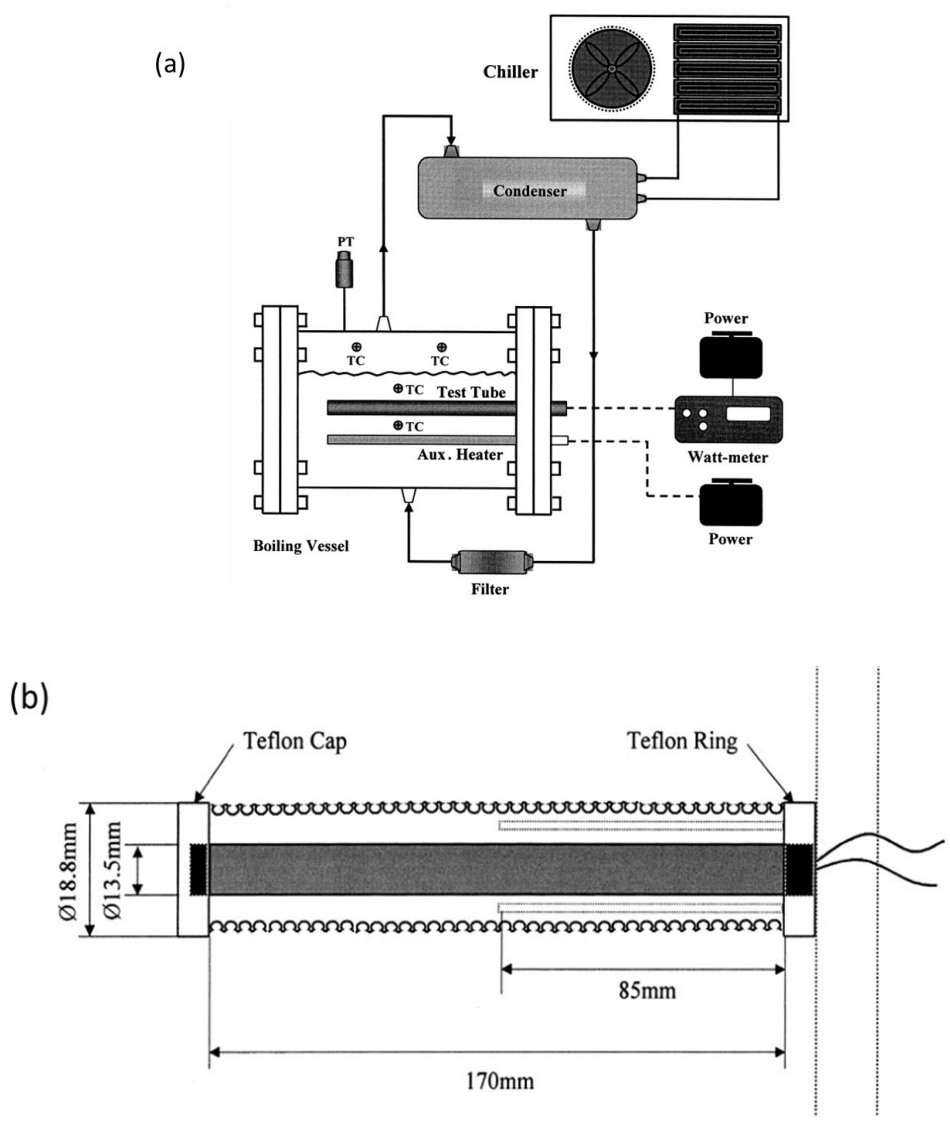

Figure 2.18: (a) Schematic drawing of experimental apparatus for pool boiling, (b) Detail sketch of the test tube [8].

Table 2.1: Summary table of available literature for pool boiling heat transfer over cylindrical samples [64].

Authors and Year	Surface Tested	Heat Flux (kW/m²)	Pressure Range (bar)	Authors and Year	Surface Tested	Heat Flux (kW/m²)	Pressure Range (bar)
Webb and Pais [65]/ 1988	Copper, R11, R12, R22, R123, R123a	3–80	1.01*	Ribatski and Jabardo [66]/ 2003	Copper, brass, stainless steel, R11, R12, R22, R123, R134a	0.6-120	1.01*
Memory et al. [67]/1992	Copper, R11, R12, R22, R123, R123a	0.5–100	1.01*	Kang [42]/2003	Stainless, water	15-90	1.01
Huebner and Kuenstler[68] /1997	Copper, n-hexane, propane	2-10	1.01	Jung et al. [69]/2004	Copper, R22, R134a, R125, R32	10-80	1.01
Chien and Webb [70] /1998	Copper, R11, R123, R123a	2-80	1.01	Chen et al. [71]/2004	Carbon steel, propane, iso-butane	2-30	1.01*
Chien and Webb [65]/ 1998	Copper, R11, R123	2-70	1.01*	Jung et al. [72]/2005	Copper, R1270, R290, R600, R600a, RE170	10-80	1.01*
Saidi et al. [73]/1999	Copper, R123	1.5-70	1.01	Ribatski and Jabardo [66]/2003	Copper, brass, stainless, R11, R12, R22, R123, R134a	0.6-120	1.01*
Kulenovic et al. [7]/ 2001	Copper, R-22, R134a, R-125, R-123	10-80	1.01*	Kotthoff et al. [74]/2006	Copper, propanol, propane	up to 100	1.01*
Kim and Choi [8]/ 2001	Copper, R22, R134a, R125, R32	Up to 50	1.01	Gorenflo et al. [75]/ 2010	Copper, R125	up to 100	1.01*
Cieslinski [76]/2001	Stainless Steel, DI water	2-1030	1.01*	Hsieh and Yang [5]/2010	Copper, R134a, R600a	0.1-30	1.01*
Kim et al. [77] /2002	Platinum, FC72	Up to 400	1.01*	Mehta and Kandlikar [64]/ 2013	Copper, water	up to 1100	1.01

Chapter 3: Motivation and Objectives

3.1 MOTIVATION

- Several different micro/nano structures have been fabricated.
- Significant increase in heat transfer has been reported during pool boiling.
- Couple of CHF models for engineered surfaces have been developed.
- The enhancement has been demonstrated.
    a. on engineered plain surfaces.
    b. using water as the boiling fluid.
    c. at atmospheric operating pressure.
- Still no general agreement on the enhancement mechanisms, let alone a universal model.
- Almost all real-world application requires curved or cylindrical surface (nuclear reactor rods, steam generators, boilers), and so far, no CHF results for engineered cylindrical surface.
- The industrial applications require high operating pressure, such as PWR 160 bars, and Steam Generators 60-80 bars, and so far, no CHF results for engineered structures on curved surfaces at high operating pressure.
- In addition to water, industrial refrigeration systems utilize various refrigerants such as FC 72, HFE liquid boiling up to 15 bar pressure, and so far, no significant enhancement has been shown for engineered structures at industrial operating conditions.
- Still no general agreement on the enhancement mechanisms, let alone a universal model Almost all real-world application require curved or cylindrical surface (nuclear reactor rods, steam generators, boilers), and so far, no CHF results for engineered cylindrical surface
- The industrial applications require high operating pressure, such as PWR 160 bars, and Steam Generators 60-80 bars, and so far, no CHF results for engineered structures on curved surfaces at high operating pressure
- In addition to water, industrial refrigeration systems utilize various refrigerants such as FC 72, HFE liquid boiling up to 15 bar pressure, and so far, no significant enhancement has been shown for engineered structures at industrial operating conditions.

- This thesis is focused on design and development of a boiling test facility to provide potential solutions to each of these issues
    a. Boiling on engineered cylindrical surfaces up to CHF (10 MW/m^2).
    b. Capable of operating up to 20 bars pressure.
    c. Can be used with both water and dielectric fluids, e.g., FC 72.

3.2 OBJECTIVES

Boiling heat transfer is widely used in many applications due to the high heat transfer that can be achieved compared to single-phase forced convection. In boiling, it can be observed the presence of two phases in thermodynamic non-equilibrium, liquid and vapor, that is the reason that pool boiling is a complex physical phenomenon. In many engineering applications quantifying the heat transfer characteristics of boiling has proven to be very difficult because all the equations used for describing this phenomenon are empirical correlations used to estimate the heat transfer characteristics with built-in margins of error. The time and money invested to get new correlations for pool boiling are very high. However, a lot of researchers are doing a great job in theoretical correlations but each research has its own idea of how to enhance pool boiling without reaching the final correlation that involve all parameters of pool boiling. So much research has to be done before researchers obtain the final correlation that describe the physical phenomenon of boiling. Newer models show more precisely the quantifying of the HTC with high HCT because they are including fundamental boiling parameters such departure time, bubble diameter, etc. These empirical correlations with boiling parameters are able to predict the failure of the surface with less error than those without an extend use of boiling parameters. Nowadays, the empirical correlations are almost based on flat surfaces with engineering modifications such as roughness, microchannels, structured surfaces, etc. Now, the goal of this thesis is to design a pool boiling facility capable of testing cylindrical engineering surfaces and obtaining in the future an empirical correlation that describes the pool boiling on cylindrical engineering surfaces. However, before

the obtention of these new predictive models and engineering applications many tests will be required in this pool boiling facility where a huge amount of engineering surfaces will be tested with several different parameters, materials, different pressure, etc. The objective of this work is to validate a design of a high-pressure high heat flux facility for the test of cylindrical engineering surfaces.

Thesis is focused on design and development of a boiling test facility to provide potential solutions to each of these issues:

Task#1: Design and manufacture a cylindrical heater capable to generate up to 10 MW/m² heat flux.

Task#2: Design and develop a condenser system capable of removing up to 10 MW/m² heat flux.

Task#3: Design and manufacture a boiling chamber.

a. Operating up to 20 bar pressure
b. Capable of operating with both water and FC 72
c. Have viewport for high-speed imaging for fundamental bubble dynamics analysis

Task#4: Develop the data acquisition system for tests.

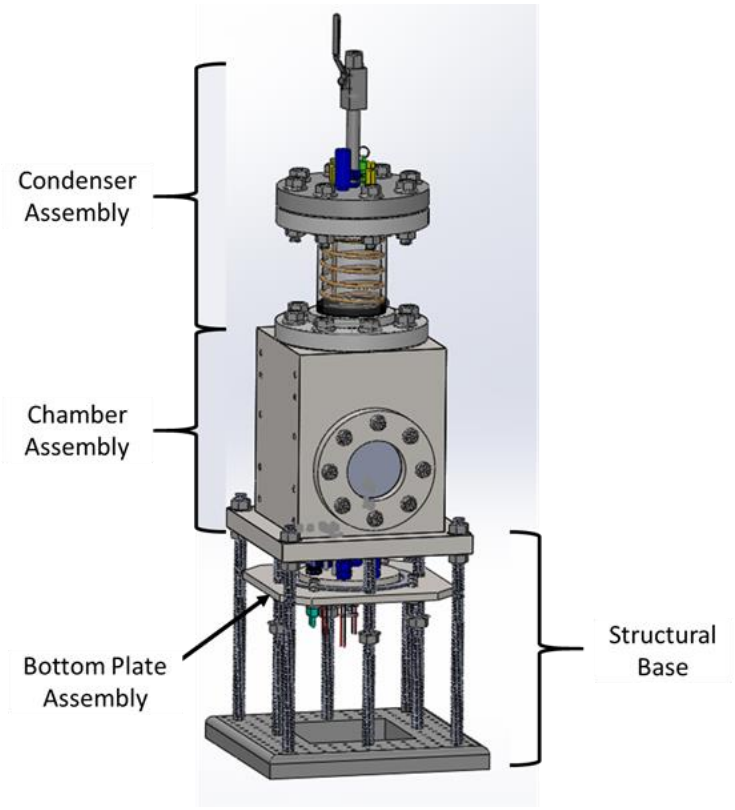

Figure 3.1: (a) Schematic Drawing of High Pressure High Heat Flux Pool Boiling Facility Four Main Assemblies.

The primary goal of this work is to design a facility capable of measuring experimental data from cylindrical engineering surfaces. To do so, a new high-pressure high temperature pool boiling facility is needed in order to conduct the experiments and collect the data with high precision and quality for an accurate validation of the physics of pool boiling models. In Fig. 3.1. It can be observed a schematic representation of high pressure high heat flux pool boiling test facility with the 4 main parts: structural Base, Bottom plate assembly, chamber assembly and, condenser assembly.

Chapter 4: Design of High Pressure High Heat Flux Pool Boiling Test Facility

The first step is designing a new test section capable to test cylindrical engineering samples. The construction of the sample heater was designed similar to the one designed by Mehta and Kandlikar [64]. The new heater incorporates changes to accommodate much higher heat fluxes, up to 10 MW/m², and the chamber can hold higher pressures of up to 10 bar. The pool boiling facility has a condensation system to control the pressure inside the chamber. The design criteria for the pool boiling facility is given in Table 4.1.

Table 4.1: Design criteria for 10 bar pressurized pool boiling.

Parameter	**Design Criteria**
Pressure	Ambient to 10 bar
Temperature	Ambient to 180 ˚C
Water Quality	DI Water
Temperature Diagnostics	Thermocouples monitoring test section in the water and steam sections. Other 4 thermocouples are monitoring the sample heater.
Pressure Diagnostics	Pressure transducer monitoring all the boiling facility.
Controls	LabVIEW for monitoring temperature and pressure.
Optical Diagnostics	Optical access through the window views.
Heat Flux	Up to 10MW/m²
Electrical Connection for Sample Heater	40 A, 95 V
Electrical Connection for Cartridge Heaters	30A, 120V

The test section will incorporate a system for cylindrical surface testing at high pressure and high heat flux and a high-speed camera on one side of the window views. The next step is to model, in ANSYS, the wall of the chamber and the window views. Finite element analyses will be performed to validate each part of this pool boiling facility design.

4.1 CYLINDRICAL HEATER DESIGN

The heater is required to produce 10 MW/m² in a cylindrical engineering sample. This sample cannot have a big diameter or length because the power requirements can go very high. The main problem for tests of this type of cylindrical engineering surface is that design of the heater is very complicated because there is not a cartridge heater capable to produce a high amount of power with these very small dimensions. The real challenge in this thesis was the design of the heater. Starting with the power requirements for the heater

Calculation for heater:

Copper rod

Specifications

Copper rod diameter: 11.6 mm

Copper length: 10 mm,

Copper rod surface area, $A = \pi d_i \mathrm{L} = 3.64 \times 10^{-4} m^2$

Required Power, P

For critical heat flux of

$q'' = 10\ MW/m^2$

$$P = q'' \times A = 3640\ W \tag{4.1}$$

Using a nichrome wire coil of 30 AWG with a resistance of 19.57 Ω/in. of coil. It is possible to play with the resistance required to define a voltage and current required to produce this amount of heat flux.

For example, let the resistance of the nichrome wire R=2.5 Ω;

$$I = \sqrt{\frac{P}{R}} = 38\ A \tag{4.2}$$

$$V = IR = 95.5\ V \tag{4.3}$$

It is possible to play with R, I, and V in order to get the desire heat flux.

4.1.1 Heater Assembly

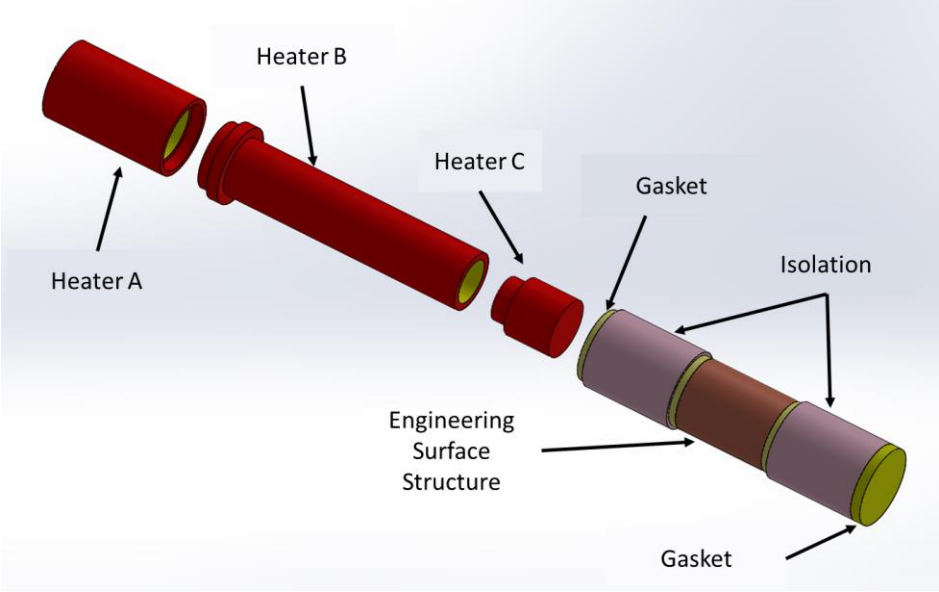

Figure 4.1: Schematic Representation of the Heater Assembly.

In Fig.4.1, it is observed the schematic representation of the heater assembly. There are five components: Heater A, Heater B, Heater C, Gaskets, Isolation and Engineering Surface structure. Heaters A, B and C are made of copper. These copper heaters get an oxidation treatment used to oxide the inside of the copper to insert the nichrome wire and avoid short circuit. After the oxidation of the three parts, it is required to remove oxide from the outside and edges of these three parts. In Fig. 4.2, it can be observed in yellow color the faces that have to remain with oxide to

avoid short circuit with the nichrome wire. Heater A is will connect with a 90˚ yor-lok fitting. The interior of this piece should keep oxide to prevent short circuit, its dimensions are 12.70 mm OD with a length of 20.86 mm, for more details see Fig. 4.3 heater A.

Heater B is the more important component of this assembly because it stores the thermocouples and nichrome wire. Its length is 45 mm and the smaller OD is 9.5mm. Heater A has the inside surface oxide to avoid short circuit, see Fig. 4.3 Heater B.

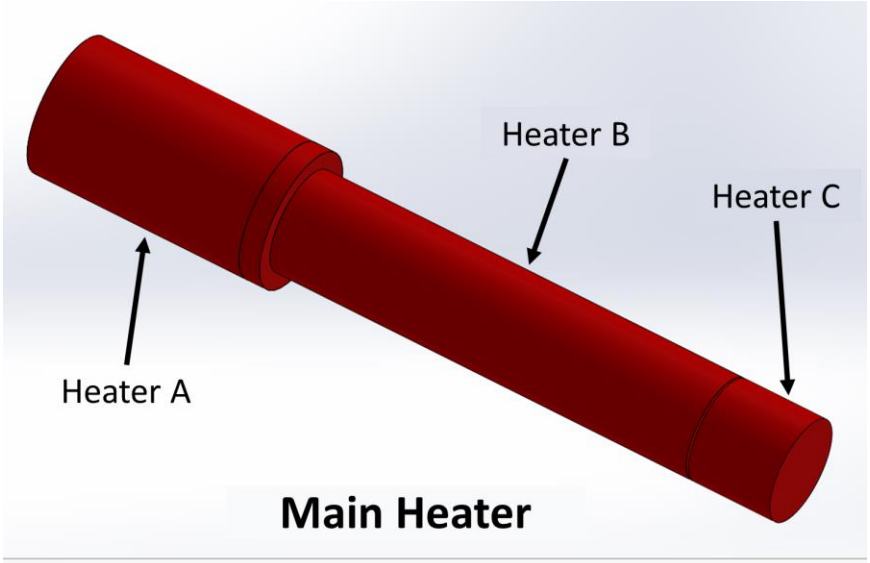

Figure 4.2: Schematic Representation of the Main Heater.

Heater C is a simple cap to seal heater A and B from the water inside the chamber. Heater B needs to have one oxide face, its total length is 11 mm with a smaller OD of 7.20 mm that will fit in Heater B, see Fig. 4.3 Heater C. After the oxidation and polishing the not required oxide faces, the nichrome wire gauge 32 AWG from Omega with a resistance of 19.57 Ω/ in of coil is installed in Heater B. Finally, the three heaters are welded with high temperature welding, this new heater is called the Main Heater, see Fig. 4.2. This Main Heater will produce the required heat flux.

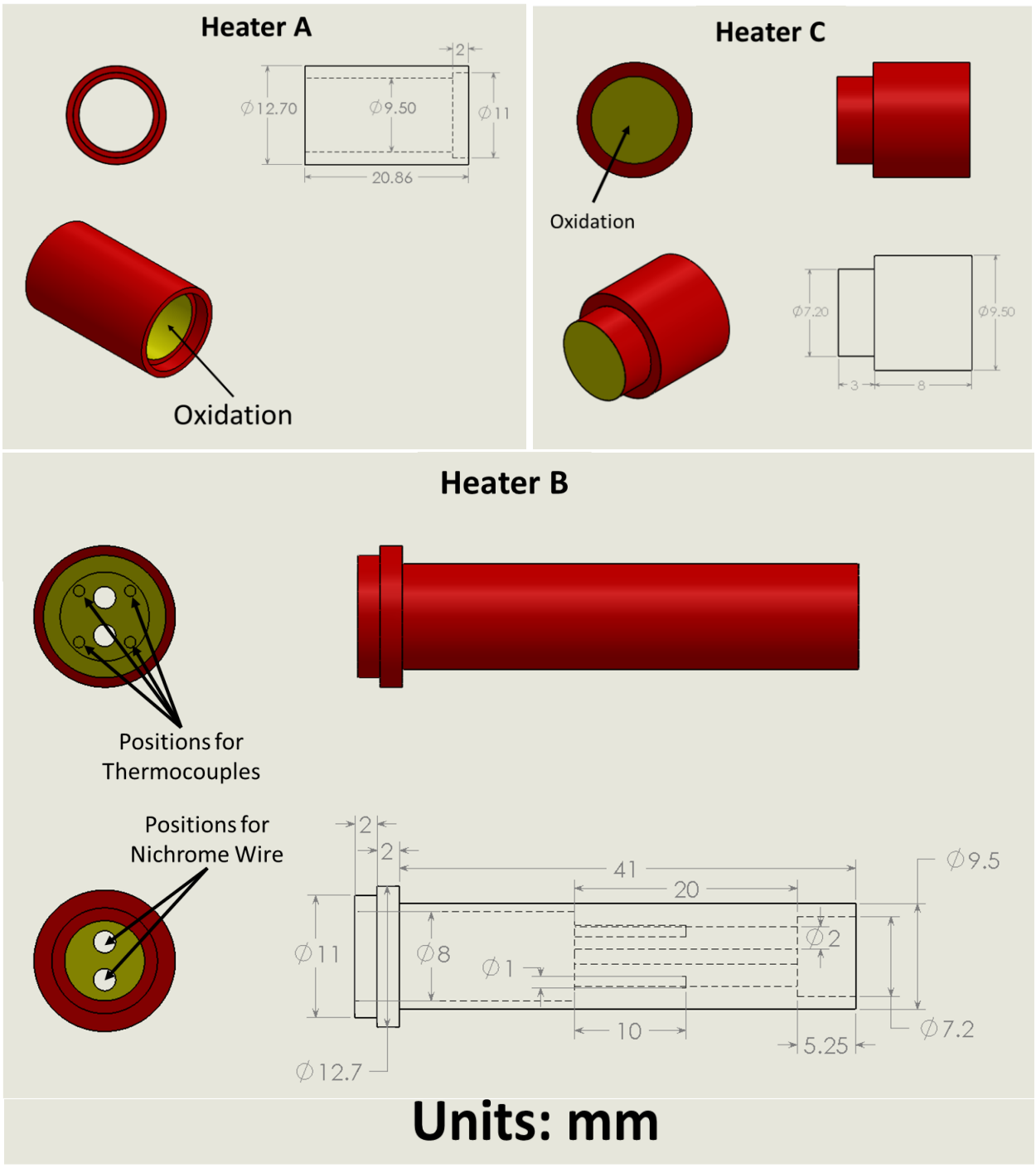

Figure 4.3: Schematic Representation of the Heater Parts.

Other components of the heater assembly are the isolation with a length of 15 mm for isolation and gaskets with 1/8” thickness. Alumina tube insolation and vermiculite gasket are used to compress the engineering sample with two compression plate. Finally, the engineering cylindrical sample has a total length of 12 mm and OD of 11.6mm.

4.1.2 Heater Thermal Analysis

A thermal analysis in ANSYS was conducted for the Main Heater with boundary conditions at exterior wall temperature of 180 ˚C and heat flux of 10 MW/m². Thermal analysis gives a max temperature of 640 ˚C and a minimum temperature of 192 ˚C, approximately. Also, it can be observed in Fig. 4.4 that all the heat will be concentrated on the position for the engineering sample. On the other hand, the distribution on the parallel plane with respect to the cylinder, the thermal distribution has a thermal isotropic distribution, this is beneficial for the measurement done for thermocouples.

Figure 4.4 shows the temperature distribution on the Main Heater, (A) is the complete heater temperature distribution where it is visible a temperature concentration in the position for the test sample. (B) represents a schematic representation of a plane parallel to the cylinder with the temperature distribution. (C) represents the face that will be welded with Heater C.

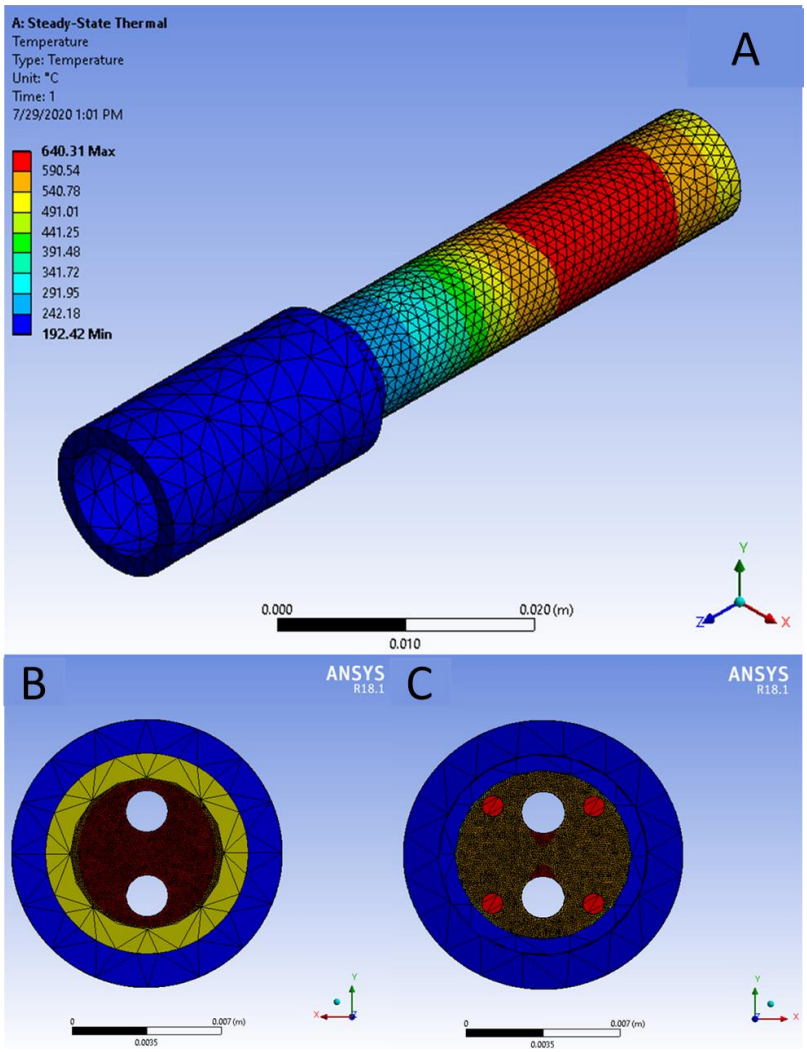

Figure 4.4: Result of finite- element Stead State Thermal Analysis for the Main Heater.

4.2 CONDENSER DESIGN

The condenser has the function of controlling the temperature and pressure condensing the steam generated by the Main Heater. In this case, the heater can setup a heat flux up to 10MW/m², the surface on the engineering sample will produce extra heat and will produce extra steam that can increase the pressure inside the chamber. For that reason, it was required to design a Coil Condenser with a cooling capacity up to 4000 W because the engineering sample with the given dimensions with a heat flux 10MW/m² will produce a power of 3640 W approximately.

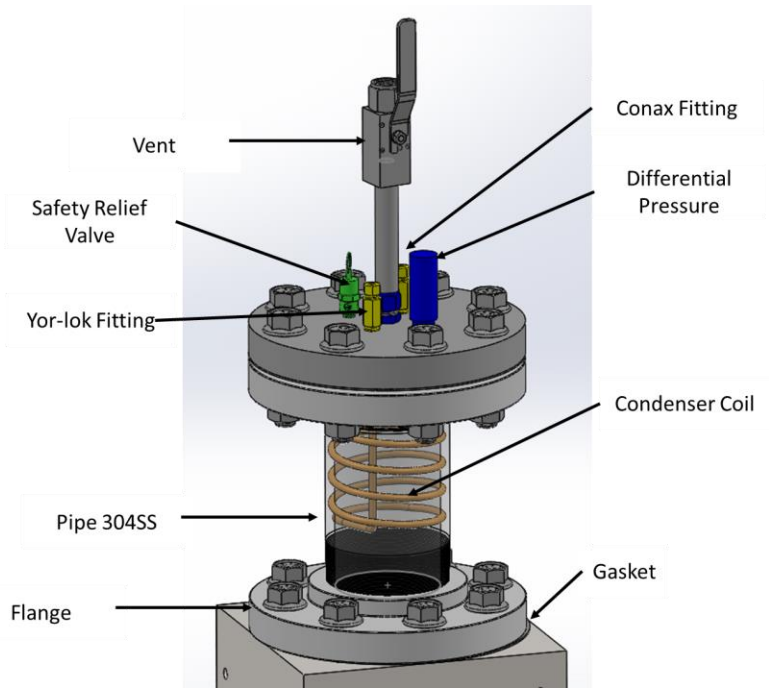

Figure 4.5: Schematic Representation of Condenser Assembly.

A schematic representation of the condenser assembly is shown in Fig.4.5. The condenser assembly has two high temperature silicone gaskets with bolt holes for 5 pipe sizes from McMaster with ANSYS Class of 150. Two threaded high-pressure pipe flanges of 304SS class 300 with 4" NPT connections are used to connect a pipe of 4" NPT made of 304 SS with length of 8 inches. Inside the pipe, there is a 3/8" OD copper coil with a total length of 0.47 m with 12 turns. On the top of the condenser assembly there is a high-pressure 304 SS unthreaded flange class 300, 4" pipe size from McMaster used for sealing the pipe. Below and on top of this unthreaded flange, there are two yor-lok fittings of 1/4" NPT placed on each side wall used for the connection of the copper coil and chiller inlet and outlet. A safety relief valve rated at 10 bar is placed on the top of the untreated flange with a high accuracy pressure transducer (item# PX01C1-300GV) with temperature range of 163 ˚C. As it is well known, saturation temperature of 10 bar is 180 ˚C, a cooling element (item# PG-CTN2-G03) from Omega was required for installing the pressure transducer in order to decrease the temperature. There is a fitting for two thermocouples of 0.125 in OD with a 1/2" NPT connection.

4.2.1 Condenser Calculations

In Table 4.2, it can be observed all the dimension for the condenser copper coil dimensions such as inner diameter d_i, outer diameter d_o, Length of the coil l, Number of Turns N, Pitch P, area of heater A_H, high of coil H.

Table 4.2: Condenser Copper Coil Dimensions.

Inner Diameter (m) d_i	**Outer Diameter (m) d_o**	**Length of coil (m) l**	**Number of Turns**	**Pitch (m) (P)**	**Area of Heater (m^2) A_H**	**High of coil (m) H**
0.007	0.0095	0.47	12	0.02m	3.64×10^{-4}	0.14

Assuming a ΔT=20˚C and a temperature in the inlet and outlet of 20 ˚C and 40˚C, respectively. The bulk temperature is defined as the average temperature of the inlet and outlet, for this calculation the bulk temperature is 20˚C.

Figure 4.6: Inlet, Outlet and Saturation Temperature at 10 bar Pressure.

A calculation for heat transfer coefficient inside the coil (h_i) has to be performed with the properties of the water at the bulk fluid, see Table 4.3

Table 4.3: Water Properties at Bulk Temperature (30˚C) and Heat Flux Conditions.

Gravity (m/s^2)	$\boldsymbol{\rho_l}$ (kg/m^3)	$\boldsymbol{\rho_v}$ (kg/m^3)	$\boldsymbol{h_{lv}}$ (J/kg)	$\boldsymbol{k_l}$ (W/mK)	μ $(Pa * s)$	$\boldsymbol{C_p}$ $\left(\frac{J}{kgK}\right)$	$\boldsymbol{Q_{req}}$ (W)	**Pr**
9.81	895	4.5	2041000	0.68	8.89×10^{-4}	4182	3640	6.99

Using a heat transfer of 10 MW/m² a total power will be 3644W. Defining the chiller conditions for $T_{in} = 20^{\circ}C$ and $T_{out} = 40^{\circ}C$ with a $T_f = 30^{\circ}C$,

$$Q = \dot{m}C_p(T_{in} - T_{out}) \tag{4.4}$$

where Q, C_p and $\dot{m}$ are the heat transfer, specific heat of water and mass flow rate, respectively. Solving for $\dot{m}$, it is obtained a mass flow rate of 0.0435 kg/s. First, it is required to calculate the Reynolds number for the definition of laminar or turbulent flow.

$$Re_i = \frac{4\acute{m}}{\pi \mu d_i} \approx 10000 \tag{4.5}$$

where μ and d_i are the dynamic viscosity and inner diameter of the coil, respectively. The flow is turbulent because $Re_i > 4000$, Now, it is required to calculate the heat transfer coefficient inside the coil h_i with Chilton-Colburn Nusselt Number Correlation.

$$Nu = 0.023Re^{0.8}Pr^{\frac{1}{3}} \tag{4.6}$$

$$\frac{h_i d_i}{k_l} = 0.023Re^{0.8}Pr^{1/3} \tag{4.7}$$

where k_l is the thermal conductivity of water. Solving for $h_i = 6800\ W/m^2K$. Using heat transfer convection equation, it is possible to calculate the T_w inside the coil.

$$Q = h_i A_i \left(T_w - T_f\right) \tag{4.8}$$

The value for T_w is 91 ˚C. Assuming the thickness of the copper coil as a very thin material with any thermal resistance. The temperature wall inside the coil can be the same outside the coil.

$$T_w = T_{w,in} = T_{w,out} \tag{4.9}$$

If the inner coil wall temperature is let as $T_{w,in}$ then the heat transfer coefficient outside the coil $\bar{h}_o$ from the condensation side can be calculate as

$$\bar{h}_o = 0.729 \left(\frac{g(\rho_l - \rho_v) k_l^3 h_{lv}}{N \mu_l \left(T_{sat} - T_{w,in}\right)} \right)^{\frac{1}{4}} \tag{4.10}$$

$$\bar{h}_o = 5132\ W/m^2$$

where $g, \rho_l, \rho_v, k_{l,} h_{lv}, N, \mu_l$ and T_{sat} are gravity, liquid density, vapor liquid, thermal conductivity, latent heat of vaporization per unit mass, coil number of turns and saturation temperature, respectively. Using heat transfer convection equation for the condensation side Q_{cond}

$$Q_{cond} = \bar{h}_o A \left(T_{sat} - T_{w,out}\right) \tag{4.11}$$

$$Q_{cond} \cong 5\ KW$$

Enough for the required heat of 3644W. The chiller from Thermo Fisher Scientific with a cooling capacity up to 5000 W is used to extract the extra heat from Eq.4.11.

4.3 HIGH PRESSURE BOILING CHAMBER

4.3.1 Structural Base

The first part to be described is the structural base that is used to support the weight of all the setup. The first item is a plate of aluminum 6061 with dimension of 15” x15” x1.5” with 1/4”-clarence holes use for insert 1/4"-20 screws to connect with an optical table. Also, there are 8 holes 3/4”-16 use for 8 rods on the aluminum plate to hold all the weight of the chamber, bottom plate, case for coil, and the condenser.

It is required to verify that these 8 rod-columns are able to hold the total load of the test facility including a safety factor of 20% of the real weight. There are three considerations for this simulation in ANSYS.

- The simulation considered 8 high strength steel rods as the columns of the experimental setup, it is important to verify the loads on it and should observe, it collapses or not.
- Thus, 4 rods (16.5 in. long) at the corners of the setup and 4 rods (15 in. long) located in a circular pattern of 9.5 in. from the center of the aluminum plate. A total force was set at 2000 N (200 Kg).
- Total deformation, von-Mises equivalent strain, deformation in Y- direction, etc. Solutions were taken and the data ad results were analyzed.

The tensile strength for these steel threaded rods is approximately 1000 MPa. Results of the finite element stress and total deformation are shown in Fig. 4.7. It can be observed that maximum von-Mises stress is less than 3Mpa (Fig. 4.7(a)) and there is a total deformation of 2.45 μm, see Fig. 4.7 (b). With these results it can be concluded that this structure base can support the total weight of the experimental facility because the maximum value for von-Mises stress is considerably below the tensile strength of these rods.

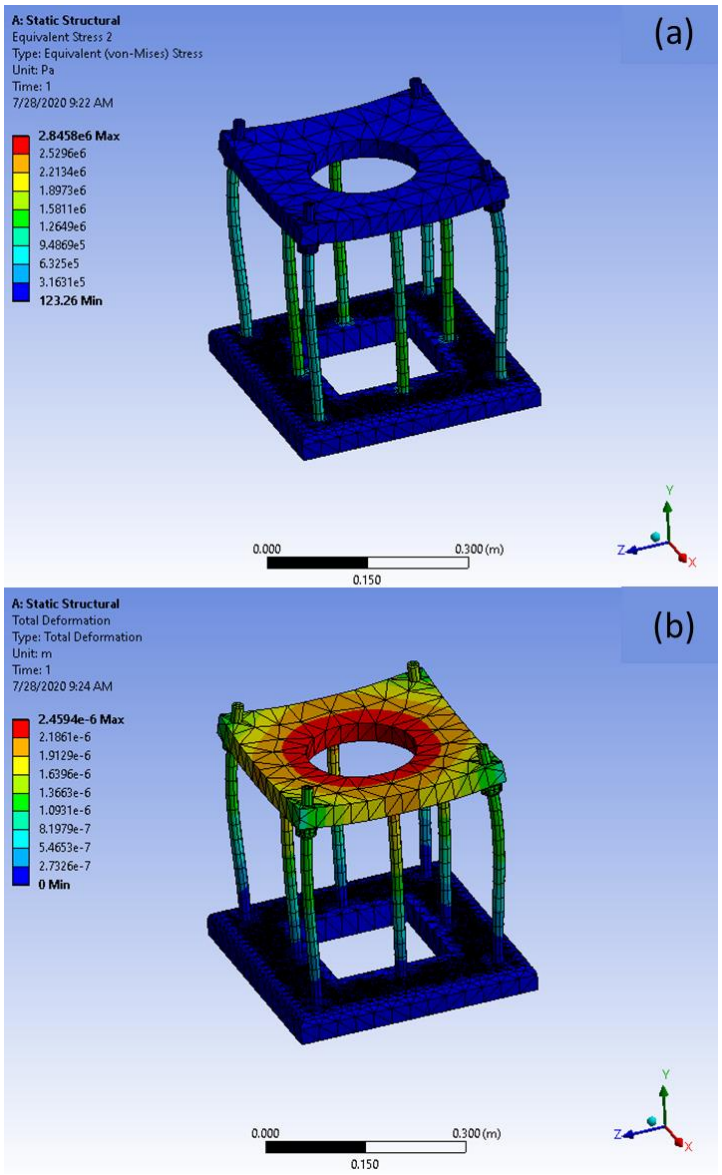

Figure 4.7: Results of Finite Element (a) Stress Analysis and (b) Total Deformation for structural base.

4.3.2 Bottom Plate for Boiling Chamber

The bottom plate assembly is located under the chamber. There is a plate made of stainless steel 304, see Fig. 4.8. It has dimensions of 12in. ×12in. × 1in. with 4 cuts in the corners at 1.7 in at 45˚ in order to avoid touching the rods from the structure base. There are 4 through holes of 5/8”-clearance holes in a circle of 9.5 inches in diameter where screws are installed for compress the bottom plate with the chamber. Additionally, 4 holes of 3/4” -clearance holes are in the same

circle where 4 rods from the structure base. The bottom plate can slide through these 4 rods. In middle of the chamber there is a extrude circle that fit in the hole under the chamber. This extruded circle has 5 holes with 1/2" NPT where Yor-lok fittings will be installed on the bottom plate. Also, two holes 3/8”-16 are used to install rods that will help to hold the engineering sample. Finally, a 1/4” NPT is used to install a draining valve on the opposite face of the extruded circle.

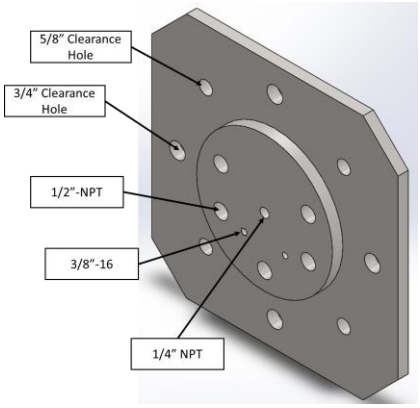

Figure 4.8: Bottom Plate and Assembly.

In Figure 3.13 presents all the components of the bottom plate assembly and it is related with Table 3.5 where it specifies all the components with part number and branch company. Item 1, represents the chamber bottom plate already described. Item 2, correspond to a draining valve with 1/4” MNPT connection, it is used for draining the chamber after the experimentation. Item 3 describes the 4 screws of 5/8”-16 with a length of 1.25 inches in length. These screws are used to compress the chamber bottom plate with the main chamber. Item 4 is a metallic gasket ANSI class 150 rated up to 150 psi, this gasket can be changed if it is required to go at high pressures because the design of the chamber can hold different diameter gaskets for different materials such as silicon, vermiculite, etc. with a high ANSY class.

There are 4 fittings for 1/2 in OD made of 316SS, see Fig. 4.9. These components are used for installing 4 heaters with a copper cover. One extra fitting is used for installing a pipe (item 8) with a 90˚elbow fitting (item 17). Item 17 is used to hold the heater assembly, see item 19 in Table 4.4. Item 6 and 7 correspond to thermocouples and electrical connections. Item 9 is called a tube

holder used to attach the compression rectangular plate to the tube. Components 12 and 13 are screws for the tube holder (item 9). Items 10 and 11 are a compression rectangular plate and a compression circular plate, respectively. These two plates compress the heater assembly with 4 screws (item 14) and nuts (item 15). Item 16 is a rod of 3/8”-16 with a length of 6 inches used for holding the compression rectangular plate (item 10).

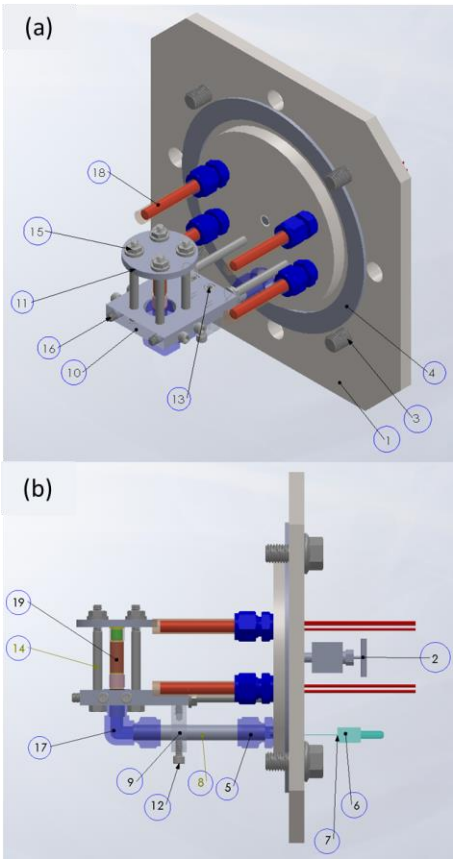

Figure 4.9: Schematic Bottom Plate Assembly.

Component 19, it is an assembly of a cartridge heater with a cylindrical cover of copper, see Fig. 4.9, the copper rod has an OD of 1/2”, this rod with the heater is installed in the yor-lok fittings (item 5). In Fig. 4.9, it can be observed a heater assembly with item number 19 in Fig. 4.10.

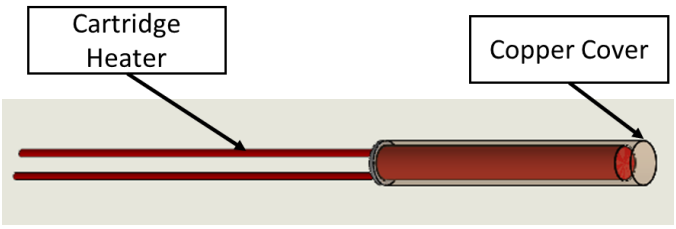

Figure 4.10: Schematic Bottom Plate Assembly.

Table 4.4: List of material of Bottom Chamber Assembly.

#	PART DESCRIPTION	QUANTITY
1	CHAMBER BOTTOM PLATE (ChBP)	1
2	DRAINING VALVE	1
3	SCREW FOR ChBP	4
4	METAL GASKET	1
5	FITTING FOR ChBP	5
6	THERMOCOUPLES	4
7	ELECTRICAL CONNECTIONS	2
8	PIPE	1
9	TUBE HOLDER	1
10	COMPRESSION RECTANGULAR PLATE	1
11	COMPRESSION CIRCULAR PLATE	1
12	SCREW FOR TUBE HOLDER	1
13	SCREW FOR REWCTANGULAR PANNEL	2
14	COMPRESSION SCREW PANNELS	4
15	NUTS DOR PANNEL COMPRESSION	4
16	ROD 3/8	2
17	ELBOW FITTING	1
18	WATER HEATER ASSEMBLY	4
19	SAMPLE HEATER ASSEMBLY	1

4.3.3 Boiling Chamber Fluid Height

The inside chamber volume was designed following the idea that inside, water of the chamber will start at ambient temperature and will be heated up to its boiling point at atmospheric pressure. After 30 minutes of rigorous boiling, the air and non-condensable gases trapped inside the chamber will be expulsed out using the degassing valve.

The main idea is after 30 minutes of vigorous boiling the volume of water must change leaving an empty space, this space has to be filled out with steam to produce the required pressure. Finally, a calculation of the amount of mass that has to be transformed from water to liquid to produce 10 bar pressure.

Degassing process

Initial volume of water 8 liters (7in x 7 in x 10 in).
Boling point T=100 °C
Vacuum time, t = 30 min= 1800s
Latent heat, L = 2256.4 KJ/kg (atm pressure)
Assuming, four cartridges of 500 W.
Total potency, P = 2000 W

In the first step, it was assumed that there is no heat lost in our system, and the temperature will be at constant boiling point (T=100 °C) with this potency.

$$Pt = mL, \quad m = \frac{Pt}{L} = \frac{(2000\ \text{W})(1800\text{s})}{2256.4\ \text{KJ/kg}} = 1.6\ kg \tag{4.12}$$

where m, t, P and L are mass, time, heat power and Latent heat, respectively. This calculation gives a mass loss of 1.6 kg of water in a vigorous boiling.

Change of high

The initial level of water is $h_1 = 10\ in$, after 30 minutes of vigorous boiling the level of water will finish in $h_2 = 8\ in.$ with a $V_{watervol} = 6.4\ litres$. Then, the change of height is:

$$\Delta h = 10\ in - 8\ in = 2\ in \tag{4.13}$$

After 30 minutes of water boiling inside the chamber, all the non-condensable gases and 1.6 kg of mass will have been taken out of the chamber with the degassing valve.

Empty Volume Inside The chamber

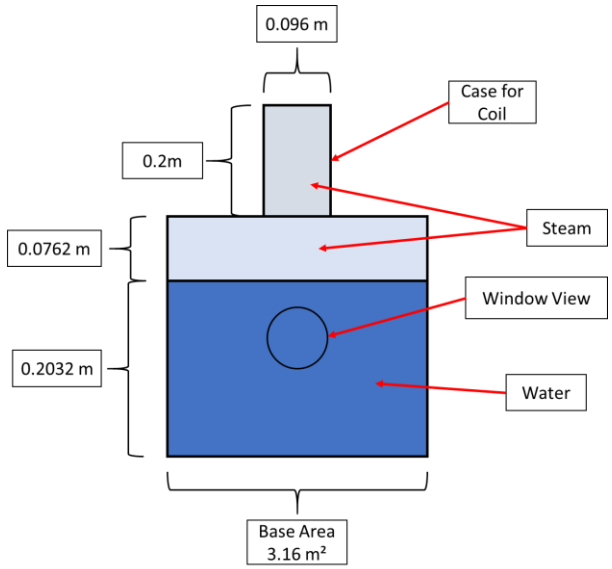

Figure 4.11: 2D CAD of the Pool Boiling Facility for High Pressure High Heat Flux for water and steam mass calculation after 30 min of vigorous boiling.

The total volume is made up of two sections, the actual chamber and the case for the coil, see Fig. 4.11. Dimensions of inside the chamber are 0.1778m × 0.1778m ×0.2794m (7 in. ×7 in. ×11in.) and for the case for coil are 0.096 meters in diameter and 0.2 m in length. Calculating the empty volume for the coil case ($V_{vapor-Cyl}$) and the empty space in the chamber (V_{vapor}).

$$V_{vapor-Cyl} = 1.44 \times 10^{-3} m^3$$

$$V_{vapor} = 0.0024\ m^3$$

Calculating the total empty space in the chamber and case for coil (V_{empty})

$$V_{empty} = V_{vapor} + V_{vapor-Cyl} \tag{4.14}$$

$$V_{empty} = 3.84 \times\ 10^{-3} m^3$$

Steam mass needed to fill the empty space inside the chamber

The total empty volume has been calculated. Now it is required to find the number of liters that will be transformed from liquid to steam and check the height of the water that will fill the cylindrical engineering sample and the window view at a pressure of 10 bar and at saturation temperature. Using ideal gas equation, it is possible to calculate the number of moles and obtain the mass of water required to fill this empty space with the pressure of 10 bar.

P=10 bar = 9.869 atm

T= 180 °C =453 K

R=0.08206 atm L/mol K

n = number of mol

V= $3.84 \times 10^{-3} m^3 = 3.84\ L$

$$PV = n\,RT \tag{4.15}$$

$$n = \frac{RT}{PV} = \frac{(0.08206\ \text{atm L/mol K})(453\ \text{K})}{(9.869\ \text{atm})(3.84\ L)} = 0.98 mol \tag{4.16}$$

For H_2O the relation is 18 g/ mol, our mass will be 17.64 grams.

Now, using other approximation with equation of Van der Waals:

$$\left(P + \frac{an^2}{V^2}\right)(V - nb) = nRT \tag{4.17}$$

Where P is pressure (9.869 atm), V volume (3.651 L), R constant of gas(0.08206 atm L/mol K), T temperature (453 K), "a" is a measure of the average attraction between particles $\left(5.46\ \frac{atm\ L^2}{mol^2}\right)$, "b" is the volume excluded by a mole of particles and finally $\left(0.0305\ \frac{L}{mol}\right)$, "n" is the number of moles. Solving for "n", it is obtained an equation of third order.

$$-n^3\frac{ab}{V^2} + n^2\frac{a}{V} + n(-Pb - RT) + PV = 0 \tag{4.18}$$

$$n = 0.95\ mol$$

It is known that 1 mol of water has a mass of 18 gr.

$$1\ mol\ H_2O \rightarrow 18\ gr\ H_2O \tag{4.19}$$

Finally, the mass of water that has to be transformed from water to steam is between 17.1 gr and 17.64 gr.

$$17.1\ gr\ H_2O \leq steam\ mass \leq 17.64\ gr\ H_2O$$

Now, it is possible to design the inside chamber with these dimensions, pressure, volume of water and steam. In the next section, it will be described the dimension and materials of the chamber and other components.

4.3.4 Chamber and View Port

The chamber plays an important role in this experimental facility because it is in charge of containing the working fluid, cylindrical test sample and has to be able to withstand the high pressure and high temperatures. by 6 plates of 304 SS with wall thickness of 1 inch and a top wall

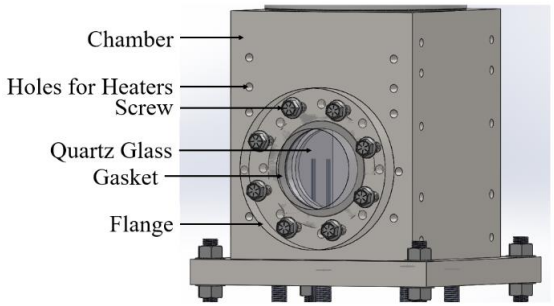

Figure 4.12: Schematic of Chamber.

thickness of 1.5 inches. The high thickness it is required to insert cartridge heaters to avoid the heat loss and to have a good look of the chamber, see Fig. 4.12. The base plate of the chamber has dimensions of 13in. × 13in. × 1in. The box has external dimensions of 10in. × 10in. × 12.5in.

with internal dimensions of 7in. × 7in. × 11in. The chamber has two window sections of 4 inches in diameter, there is one entry on the bottom used for installing the bottom plate assembly (describe in section 4.5) with a hole diameter of 6.67 inches. and there is a hole in the top of the chamber used to connect the condenser system with the chamber with a hole diameter of 3.83 inches that correspond to the inner diameter of a 304SS pipe used in the condenser. There are 18 holes of 3/8"-clearance holes use for insert the cartridge heaters for heat loss. The length of these heaters is 8 inches and 1.5 inches.

There are two window sections, each section has a quartz glass, a metal gasket and a flange of 304 SS. Quartz glass is from Machined Glass Specialist, it has dimensions of 4.375 inches in diameter and 1.125 inches in thickness, it is compress with a gasket and a flange using 8 screws 1/2”-20, see Fig. 4.13.

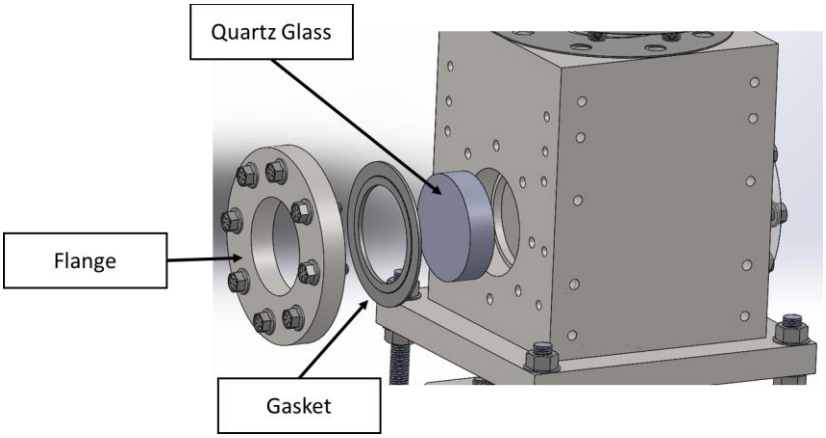

Figure 4.13: Chamber with Window View Section.

A finite stress and total deformation analysis were performed for the quartz glass windows using a safety factor of 2 for a pressure on the quartz glass of 40 bar. The tensile stress for quartz is 50 MPa. After the simulation analyses the max von-Mises stress is closed to 45 MPa, and there is a total deformation of 8 μm, see Fig.4.14.

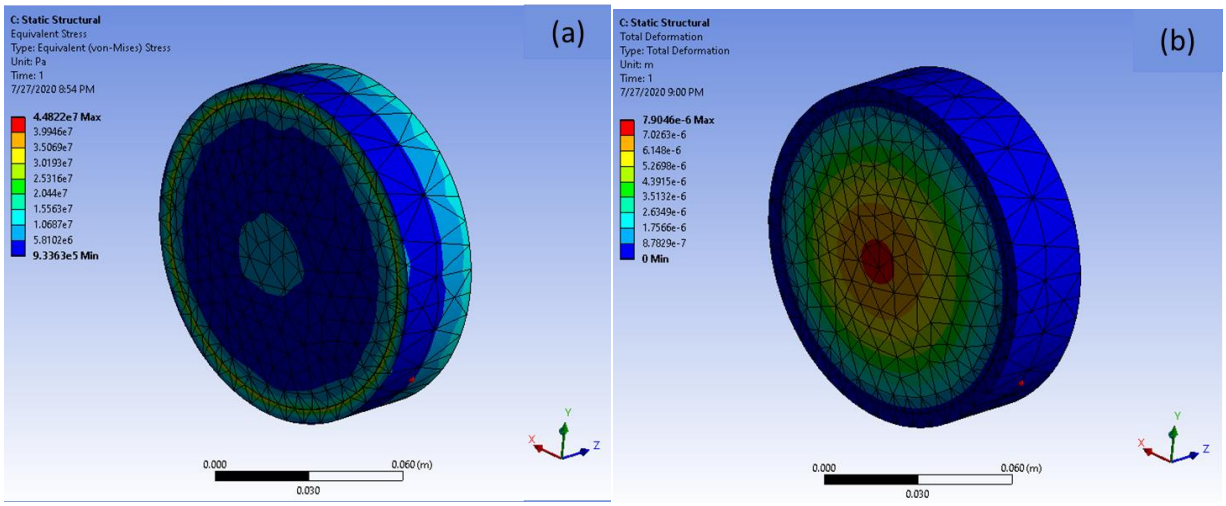

Figure 4.14: Results of Finite Element (a) Stress Analysis and (b) Total Deformation for quartz.

4.3.5 Chamber Wall Heating

There are 3 sections where the use of heaters 3/8” diameter from West Cost Plastics are required.

- Water Bath: There are 4 heaters on the Bottom Plate Assembly, see Section 3.6. They are used for heat the water up to saturation temperature, these heaters have a power of 500 W, 120 V with dimensions of 2 in length and 3/8” diameter.
- Steam-Wall: There are 6 heaters with a power of 600 W, 120 V and 2 heaters with a power of 1000W located around chamber side top wall use to heat the steam up with a length of 8 in.
- Water-Wall: There are 8 small heaters of 1.5 in. in length with a power of 250W next to the window section, and 8 heaters with a length of 8 in. with a power 600W located around chamber bottom side wall.

Steam-Wall and Water-Wall heaters are located inside the chamber’s holes to offset the heat loss from the inside wall to the outside wall. In Fig. 4.15, it is represented the heaters circuit diagram.

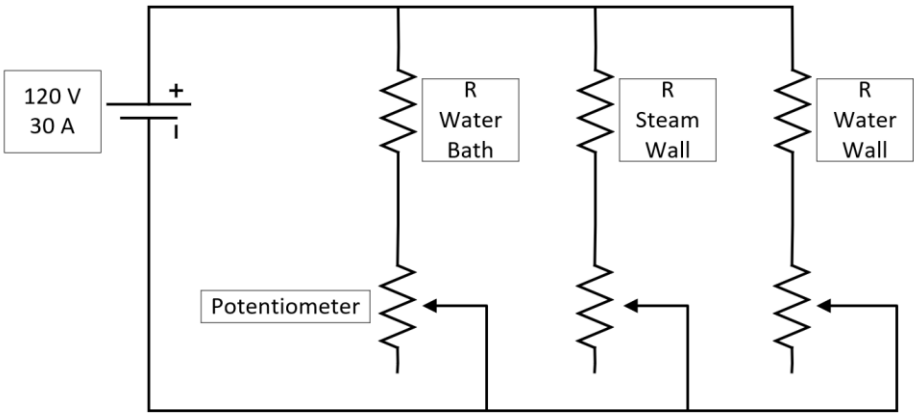

Figure 4.15: Heaters Circuit Diagram.

It is well known that a heater should not work at its 100% capacity. For that reason, it was conducted an analysis for current (I), voltage (V) and resistance (R). For each section, it was calculated the individual max current allowed with a 120V AC.

Heaters Analysis

- Water Bath has 4 heaters

Features of an individual heater: 500W and 120V.

Using Ohm's Law it is possible to calculate the current and resistance used for each individual heater at 120V.

$$I = \frac{P}{V} = \frac{500W}{120V} = 4.16A \tag{4.20}$$

$$R = \frac{V}{I} = \frac{120V}{4.16A} = 28.84\ \Omega \tag{4.21}$$

Now, it is required to calculate the total resistance for water bath (R_{WB}) for a parallel circuit with 4 heaters.

$$R_{WB} = \frac{28.84\ \Omega}{4} = 7.21\ \Omega \tag{4.22}$$

$$I_{wB} = \frac{V}{R} = \frac{120V}{7.21\Omega} = 16.64\ A \tag{4.23}$$

where I_{wB} is the total current. This same analysis was performed in for Steam-Wall and Water-Wall.

- Steam-Wall has 8 heaters.

Features of an individual heater: 6 heaters with 600W,120V and 2 heaters with 1000W,120V.

Using Eq 4.1and 4.2 to calculate individual current and resistance.

Heaters with 600 W current and resistance:

$I = 5A$
$R = 24\ \Omega$

Heaters with 1000 W current and resistance:

$I = 8.33A$
$R = 14.4\ \Omega$

Total resistance for steam-wall (R_{SW}) for a parallel circuit with 6 heaters of 600W and 2 heaters of 1000W:

$$R_{sw} = R_{sw,6} + R_{sw,2} = \frac{24\ \Omega}{6} + \frac{14.4\ \Omega}{2} = 11.2\ \Omega \tag{4.24}$$

$$I_{sw} = \frac{V}{R} = \frac{120V}{11.2\Omega} = 10.71A \tag{4.25}$$

where $R_{sw,8l}$, $R_{ww,2s}$ and I_{sw} correspond to the resistance for 8 heaters with 600W, resistance for 2 heaters with 250W and total current for the parallel circuit, respectively.

- Water-Wall has 16 heaters.

Features of an individual heater: 8 heaters with 600W,120V and 8 heaters with 250W,120V.

Using Eq 4.1and 4.2 to calculate individual current and resistance.

Heaters with 600 W current and resistance:

$I = 5A$
$R = 24\ \Omega$

Heaters with 250 W current and resistance:

$I = 2.08A$
$R = 57.69\ \Omega$

Total resistance for steam-wall (R_{ww}) for a parallel circuit with 6 heaters of 600W and 2 heaters of 1000W:

$$R_{ww} = R_{ww,8l} + R_{ww,8s} = \frac{24}{8} + \frac{57.69}{8} = 10.21\Omega \quad (4.26)$$

$$I_{ww} = \frac{V}{R} = \frac{120V}{10.21\Omega} = 11.75A \quad (4.27)$$

Where $R_{ww,8l}$, $R_{ww,8s}$ and I_{ww} correspond to the resistance for 8 heaters with 600W, resistance for 8 heaters with 250W and total current for the parallel circuit, respectively.

In Table 4.5, it is observed the total current used for different capacity percentages of the heaters at 120V.

Table 4.5: Total current at different working capacity percent of the heaters at 120 V.

% of Capacity	I_{WB}	I_{SW}	I_{WW}	**Total Current (Amps)**
100	16.64	10.71	11.75	39.1
75	16.64	8.03	8.81	33.48
60	16.64	6.42	7.05	30.11
50	16.64	5.35	5.87	27.87

4.4 DATA ACQUISITION SYSTEM

Any experimental test facility needs a system of data acquisition and this is not the exception. A very basic system of measurement is required for this high-pressure high heat flux pool boiling test facility for measure, see Fig.4.16.

- Temperature measurements for Steam.
- Temperature measurements for Water.
- Temperature measurements for Heater.
- Heat flux measurements.
- Pressure measurements.
-

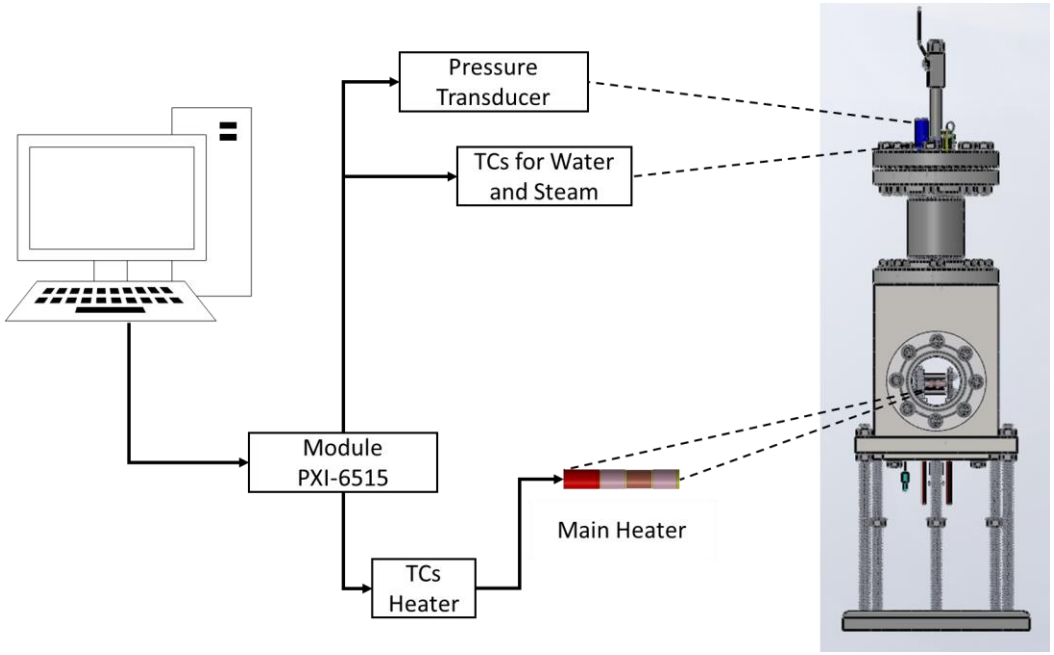

Figure 4.16: Data Acquisition Diagram.

Chapter 5: Manufactory and Assembly of High-Pressure High Heat Flux Pool Boiling Test Facility Manufactory and Assembly

5.1 Cylindrical Heater Manufactory and Assembly

The cylindrical heater is made of copper (super- conductivity) from McMaster, see Table 5.1. I was manufacture in UTEP machine shop. In Fig. 5.1, The complete assembly is shown with nichrome wire (Table 5.2), alumina tube (Table 5.3) and electrical wire. The nichrome wire is inside the cylindrical heater, see Chapter 4.

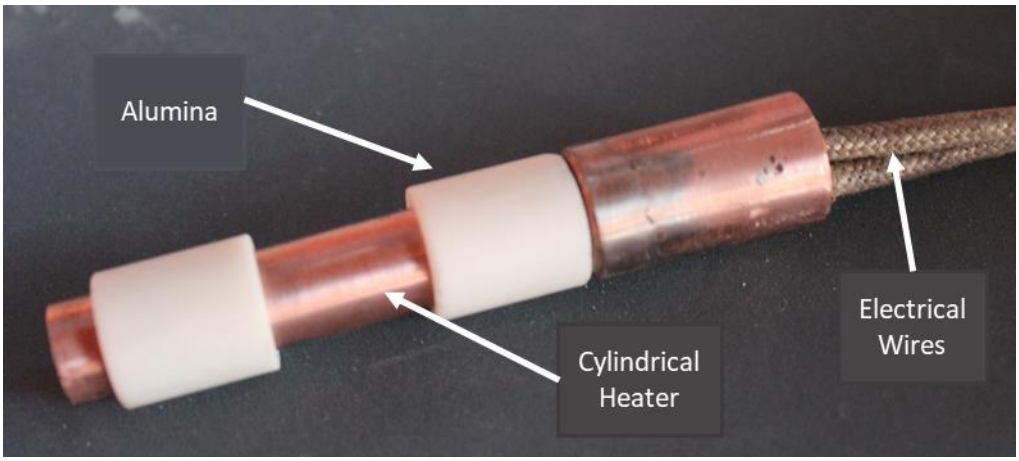

Figure 5.1: Cylindrical heater assembly.

Table 5.1: Features of copper for cylindrical heater.

Description	Specification
Material	101 Copper
Diameter	½ in
Melting point temperature	1981 ˚F
Thermal conductivity	226 Btu/hr.x ft/ ˚F
Part Number	8965K82
Company	McMaster

Table 5.2: Features for nichrome wire.

Description	Specification
Material	Nichrome wire (80% Nickel, 20% Cr)
Coil diameter	0.125 in
Wire diameter	0.01 in
AWG	30
Part Number	NIC80-010-125-100
Company	Omega

Table 5.3: Features for alumina tube.

Description	Specification
Material	Alumina ceramic
Diameter	½ in OD, 3/8 in ID
Max temperature	3075 ˚F
Part Number	8746K412
Company	McMaster

5.2 Condenser Manufactory and Assembly

Condenser was manufacture in UTEP machine shop using two threaded flange of 4" (Table 5.4), one flange unthreaded 4" (Table 5.5), 4" diameter stainless steel pipe (Table 5.6), copper coil (Table 5.7), yor-lok fittings (Table 5.8), metal barbed hose fittings (Table 5.9), relief valve (Table 5.10), cooling element (Table 5.11), degassing valve (Table 5.12), and conax fitting for thermocouples (Table 5.13). The complete assembly is shown in Fig. 5.2.

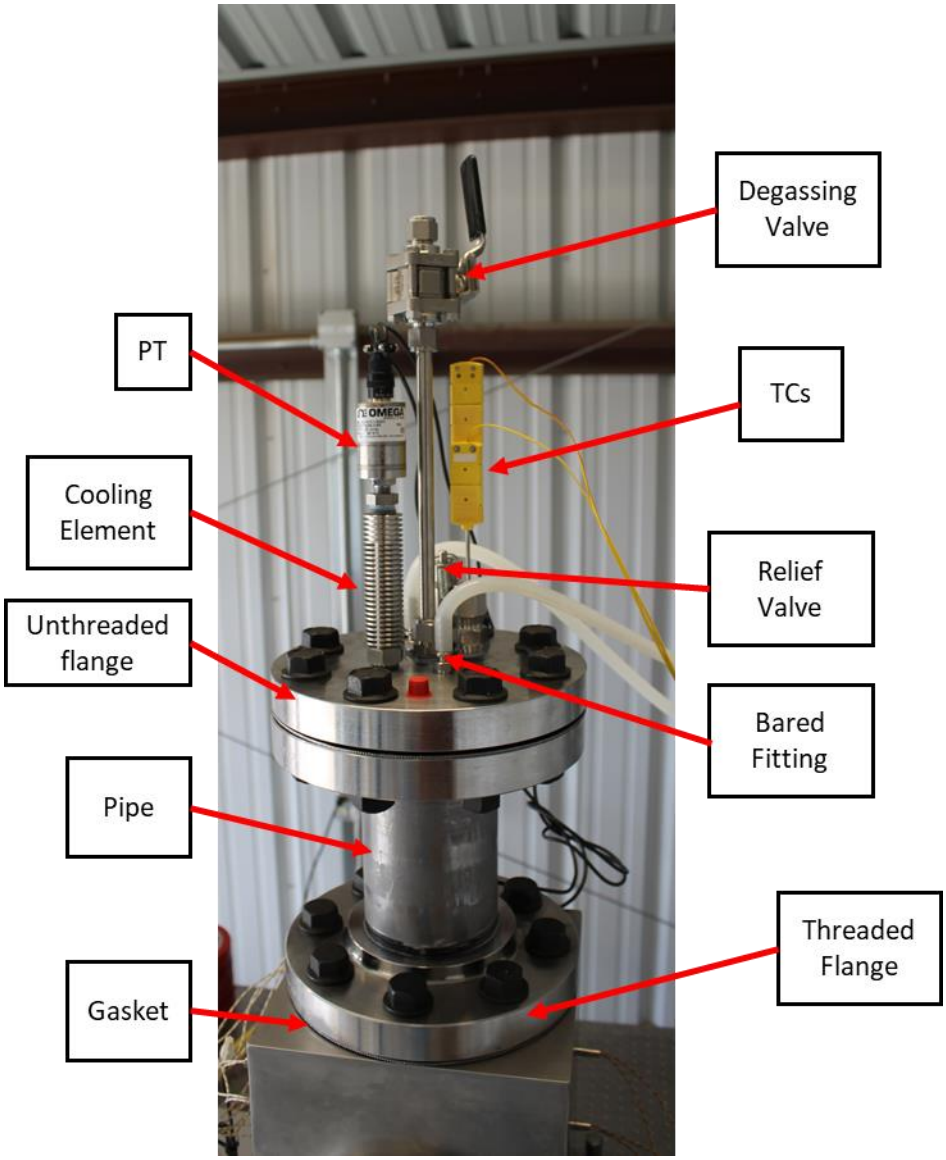

Figure 5.2 Condenser assembly.

Table 5.4: Features for threaded flange.

Description	Specification
Material	304 SS
Type	Flange/Adapter
Class	300
Number of holes and dimensions	8, 0.875 in
Part Number	7977K19
Company	McMaster

Table 5.5: Features for unthreaded flange.

Description	Specification
Material	304 SS
Type	Flange/Cap
Class	300
Number of holes and dimensions	8, 0.875 in
Part Number	4448T284
Company	McMaster

Table 5.6: Features for stainless steel pipe.

Description	Specification
Material	304/304L Stainless Steel
Schedule	80
Threading	Threaded on Both Ends
Pipe Size	4
Part Number	46755K276
Company	McMaster

Table 5.7: Features for copper coil.

Description	Specification
Material	Copper
Diameter	3/8 in OD, 0.032 in ID
Max temperature	400 ˚F
Part Number	5174K23
Company	McMaster

Table 5.8: Features for yor-lok fitting.

Description	Specification
Material	Stainless Steel
Maximum Pressure	2,000 psi @ 72° F
Type	Adapter
Temperature Range	-420° to 1200° F
Part Number	5182K133
Company	McMaster

Table 5.9: Features for metal barbed hose fittings.

Description	Specification
Material	Stainless Steel (SS)
Temperature Range	-40° to 350° F
Pipe Size	½ NPT
Part Number	5361K84
Company	McMaster

Table 5.10: Features for relief valve

Description	Specification
Material	101 Copper
Pipe Size	1/4 in NPT
Set Pressure	300 psi
Temperature Range;	-40° to 400° F
Part Number	98905K15
Company	McMaster

Table 5.11: Features for cooling element.

Description	Specification
Material	316L SS
Max temperature	300°C
Wire diameter	0.01 in
Maximum Pressure	5000 psi
Part Number	PG-CTN2-G03
Company	Omega

Table 5.12: Features for degassing valve.

Description	Specification
Material	316 Stainless Steel
Connection	½ in tubing fitting
Max temperature	232°C
Max Pressure	2200 PSIG
Part Number	SS-63TS8
Company	Swagelok

Table 5.13: Features for conax fitting for thermocouples.

Description	Specification
Material	304 SS
Connection	½ in NPT
Thermocouple connection	0.125 in OD
Part Number	C428-1
Company	Conax Technologies

5.3 High Pressure Boiling Chamber

5.3.1 Structural Base Manufactory and Assembly

Structural base (Fig.5.3) was manufacture in UTEP machine shop with an aluminum plate (Table 5.14) and ¾ in threaded rods (Table 5.15).

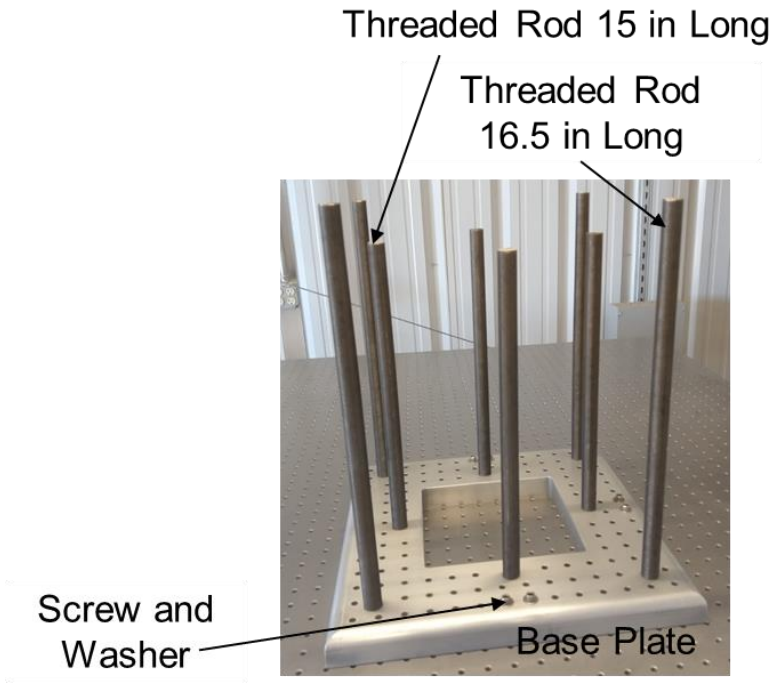

Figure 5.3 Structural base.

Table 5.14: Features for aluminum base.

Description	Specification
Material	6061 Aluminum
Connection	½ in tubing fitting
Yield Strength	35,000 psi
Temperature Range	-320° to 300° F
Part Number	89155K17
Company	McMaster

Table 5.15: Features for ¾ in threaded rods.

Description	Specification
Material	Steel
Thread Size	3/4"-16 UNC
Tensile Strength	150,000 psi
Part Number	90322A202
Company	McMaster

5.3.2 Bottom Plate for Boiling Chamber Manufactory and Assembly

Bottom plate is made of 304 SS, it was manufacture in UTEP machine shop, there are fitting of ½ in tubing straight and 90 degrees (Table 5.16), there are 4 copper cover for cartridge heater to avoid the shot circuit. There are 2 compression plates made of 304 SS, here the heater and sample will be compress for these two plates. There is tube holder made of 304 SS that they are hold with screw of SS 8-36 thread size. The total assembly is shown in Fig. 5.4.

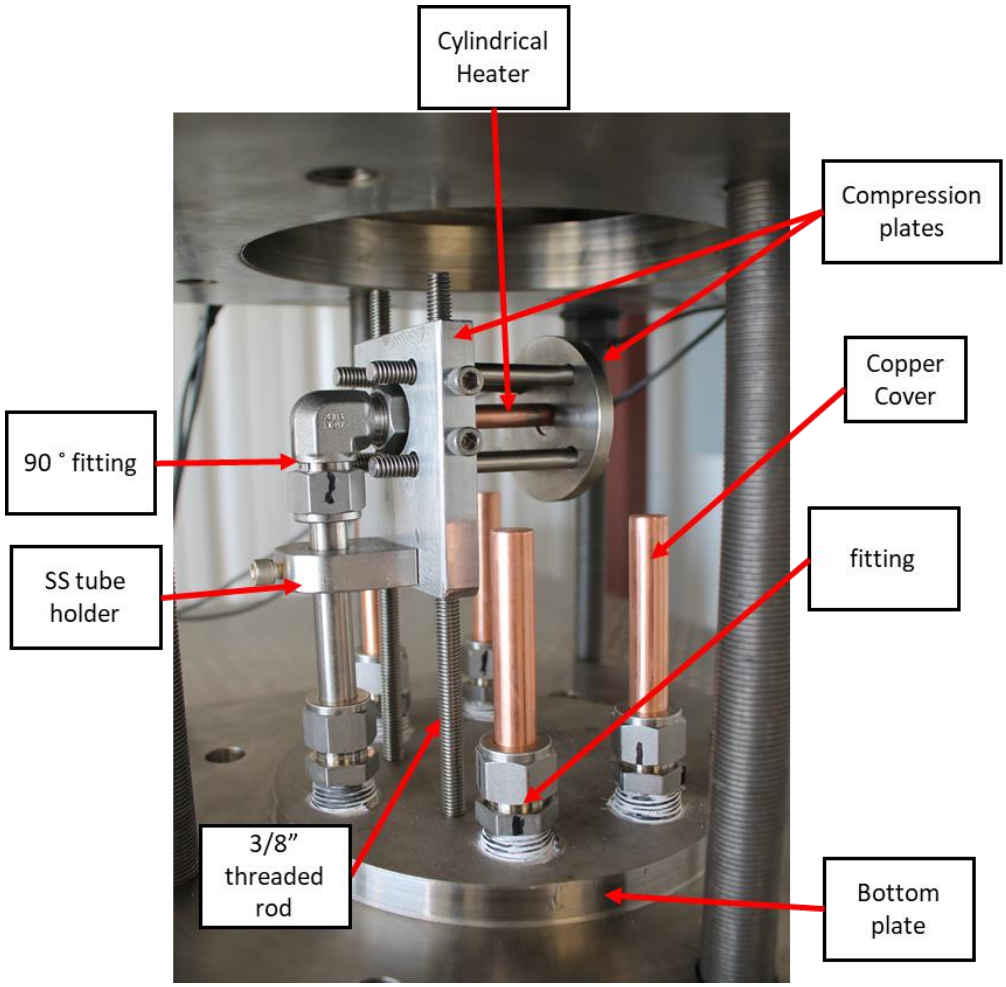

Figure 5.4 Bottom plate assembly.

Table 5.16: Features for fittings.

Description	Specification
Material	316 Stainless Steel
Connection	½ in tubing fitting (90˚ and straight)
Max temperature	232°C
Max Pressure	2200 PSIG
Part Number	SS-810-9 and SS-810-1-8
Company	Swagelok

5.3.3 Boiling Chamber and View Port Manufactory and Assembly

The boiling chamber was manufacture in Lark Industries, El Paso TX. It is made of 304SS. the complete assembly has a quartz glass (Table 5.17) of 4.125 diameter with a thickness of 1in, it has a flange made of 304 SS with 8 in OD, 4 in ID and a thickness of 1 in. The flange compresses the quartz glass with a metal gasket (Table 5.18) and it is screw with 8 screw of 1/2in-20 UNF. The complete assembly of the boiling chamber is presented in Fig.5.5. There are different dimensions for cartridge heaters with different lengths and power features, see Table 5.19.

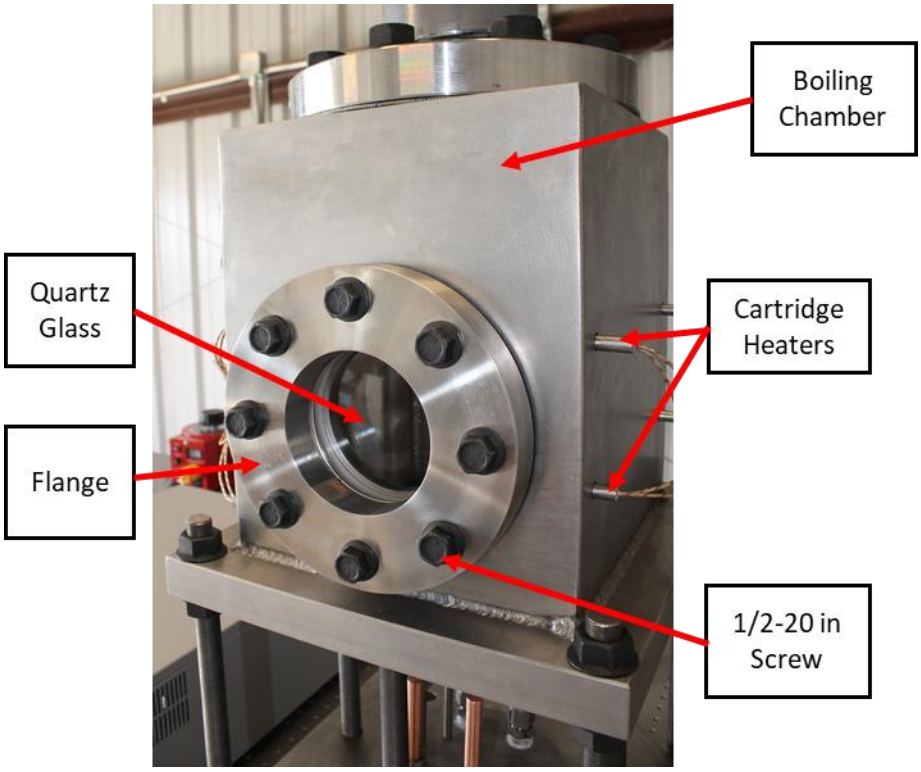

Figure 5.5 Bottom plate assembly.

Table 5.17: Features for quartz glass.

Description	Specification
Material	Quartz glass
Tensile strength	50 N/mm2
Max temperature	1080°C
Company	Heraeus

Table 5.18: Features for metal gasket.

Description	Specification
Material	SS and Graphite Filler
Dimension	4” ID, 5.875” OD, thickness 1/8”
Maximum Pressure	300 psi
Temperature Range	Temperature Range -50° to 840° F
Max Pressure	300 psi
Part Number	44955K178
Company	McMaster

Table 5.19: Features for cartridge heaters.

Description	Specification
Material	Stainless Steel
Diameter	3/8 in
G1J86-N6H	8 units
G2A95-N6H	4 units
G8A53-N6H	16 units
Company	West Cost Plastic

5.4 DATA ACQUISITION SYSTEM

Data system acquisition has a National Instruments PXI-6515 DAQ module of 32 inlets and 32 outlets from National Instruments. A SCB-100A shielded I/O connector block is use to connect all the wire of the thermocouples and pressure transducer to the DAQ module. LabVIEW is used to display and record all the measurements. The next devises where used for measure temperature, heat flux and pressure, see Table 5.20-5.23 for details. Fig. 5.6 show the devices use for data acquisition.

- Temperature measurements for Steam with a TC type K with a 0.125 in OD.
- Temperature measurements for Water with a TC type K with a 0.125 in OD.
- Temperature measurements for Heater with 4 TCs type K of 0.02 in OD.
- Heat flux measurements
- High Accuracy Pressure transducer, 0-300 psi.

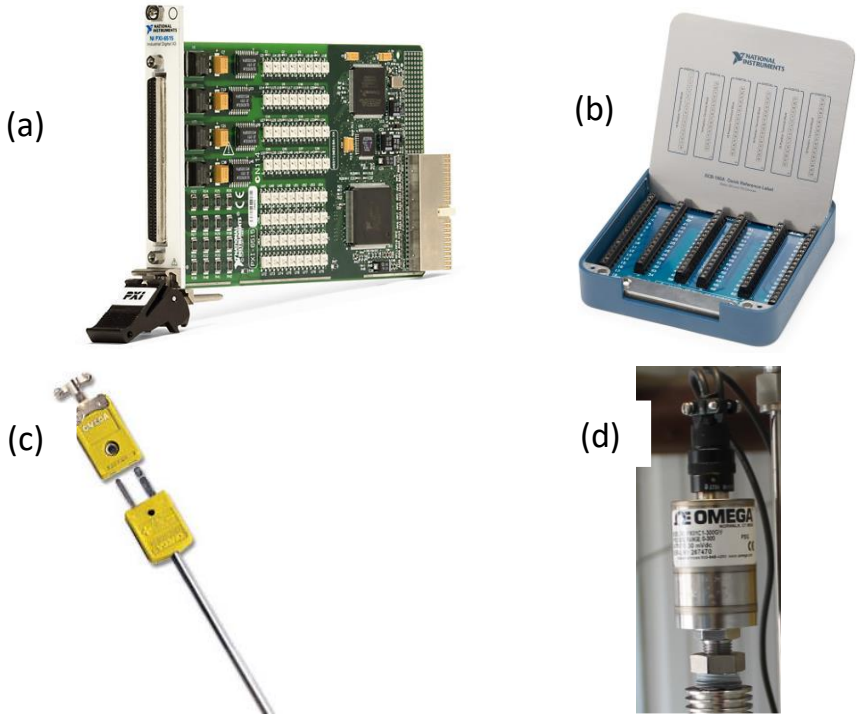

Figure 5.6: (a) PXI-6515 DAQ module, (b) connector block, (c) thermocouple type K, and (d) Pressure transducer. [78][79].

Table 5.20: Features for PXI-6515 DAQ module.

Description	Specification
Inputs	32 source/sink
Outputs	32 sink
Connector type	100-pin keyed female SCSI
Part Number	PXI-6515
Company	National Instruments

Table 5.21: Features for connector block.

Description	Specification
Minimum wire gauge	30 AWG
Maximum wire gauge	16 AWG
Connection	100
Part Number	SCB-100A
Company	National Instruments

Table 5.22: Features for thermocouple type K.

Description	Specification
Material	Stainless Steel (SS)
Temperature Range	0 to 800° C
Sensor application	Immersion Probe
Part Number	SCAXL-020U-18, KQSS-18U-12, KQSS-18U-24
Company	Omega

Table 5.23: Features for Pressure transducer.

Description	Specification
Material	101 Copper
Pipe Size	1/4 in NPT
Set Pressure	300 psi
Temperature Range;	-73 to 163° F
Part Number	PX01C1-300GV
Company	Omega

Fig. 5.7 shows the final assembly for high pressure high heat flux pool boiling test facility with the DC power supply from Chroma (DC source 100VDC/100A/5000W) use for give the power to the cylindrical heater.

Figure 5.7: High Pressure High Heat Flux Pool Boiling Test Facility Assembly.

Chapter 6: Conclusions

Literature and test facilities review has been performed in order to obtained information of the available pool boiling test facilities around the world and to have a widely knowledge of the types of engineering enhancement that it has been done in these last decades for CHF enhancement.

The design of a novel and unique heater capable to work up to 10 MW/m² has been made. After thermal and electrical analyses, the cylindrical heater is capable to produce the desired CHF of 10 MW/m².

A calculation and design for water and steam volume for 10 bar pressure was performed given the real values for water mass and steam mass for create a 10 bar pressure inside the boiling chamber.

The design of a chamber view port has been performed with structural analysis and design for a high-speed camera. After the analyses the design proves that this port view will be able to hold the pressure of 10 bar.

A design of a condenser capable to remove 10 MW/m² inside the chamber was calculated after a lot proof and error. Finally, the dimension and cooling capacity of the coil fit on the pipe of 4 in diameter.

A data acquisition system for measure temperature, pressure and heat flux was design and the devises were carefully selected to fulfil the requirements of the high pressure high heat flux pool boiling test facility to complete with the task of collect the measurements of this experimental test.

References

[1] S. Nukiyama, "The maximum and minimum values of the heat Q transmitted from metal to boiling water under atmospheric pressure," *Int. J. Heat Mass Transf.*, vol. 9, no. 12, pp. 1419–1433, 1966.

[2] P. J. Berenson, "Experiments on pool-boiling heat transfer," *Int. J. Heat Mass Transf.*, vol. 5, no. 10, pp. 985–999, 1962.

[3] K. Suzuki, K. Yuki, and M. Mochizuki, "Application of Boiling Heat Transfer to High-Heat-Flux Cooling Technology in Power Electronics," *Trans. Japan Inst. Electron. Packag.*, vol. 4, no. 1, pp. 127–133, 2011.

[4] K. H. Chu, R. Enright, and E. N. Wang, "Structured surfaces for enhanced pool boiling heat transfer," *Appl. Phys. Lett.*, vol. 100, no. 24, 2012.

[5] I. C. BANG, J. BUONGIORNO, L.-W. HU, and H. WANG, "Measurement of Key Pool Boiling Parameters in Nanofluids for Nuclear Applications," *J. Power Energy Syst.*, vol. 2, no. 1, pp. 340–351, 2008.

[6] J. S. Mehta and S. G. Kandlikar, "Pool boiling heat transfer enhancement over cylindrical tubes with water at atmospheric pressure, Part II: Experimental results and bubble dynamics for circumferential V-groove and axial rectangular open microchannels," *Int. J. Heat Mass Transf.*, vol. 64, pp. 1216–1225, 2013.

[7] R. Kulenovic, R. Mertz, and M. Groll, "High speed flow visualization of pool boiling from structured tubular heat transfer surfaces," *Exp. Therm. Fluid Sci.*, vol. 25, no. 7, pp. 547–555, 2002.

[8] N. H. Kim and K. K. Choi, "Nucleate pool boiling on structured enhanced tubes having pores with connecting gaps," *Int. J. Heat Mass Transf.*, vol. 44, no. 1, pp. 17–28, 2001.

[9] K. Stephan and M. Abdelsalam, “Heat-transfer correlations for natural convection boiling,” *Int. J. Heat Mass Transf.*, vol. 23, no. 1, pp. 73–87, 1980.

[10] K. Debache *et al.*, “Vaccination with recombinant NcROP2 combined with recombinant NcMIC1 and NcMIC3 reduces cerebral infection and vertical transmission in mice experimentally infected with Neospora caninum tachyzoites,” *Int. J. Parasitol.*, vol. 39, no. 12, pp. 1373–1384, 2009.

[11] L. Zhang, E. N. Wang, K. E. Goodson, and T. W. Kenny, “Phase change phenomena in silicon microchannels,” *Int. J. Heat Mass Transf.*, vol. 48, no. 8, pp. 1572–1582, 2005.

[12] M. M. Rahman, “Boiling Enhancement on Engineered Surfaces,” *Drexel Univ.*, 2016.

[13] C. E. Brennen, *Cavitation and bubble dynamics*, no. October. 2013.

[14] Y. Y. Hsu, “On the size range of active nucleation cavities on a heating surface,” *J. Heat Transfer*, vol. 84, no. 3, pp. 207–213, 1962.

[15] S. K. Das, N. Putra, and W. Roetzel, “Pool boiling characteristics of nano-fluids,” *Int. J. Heat Mass Transf.*, vol. 46, no. 5, pp. 851–862, 2003.

[16] V. P. Carey, “Liquid-Vapor Phase-Change Phenomena,” *Hemisph. Publ. Corp.*, 1992.

[17] A. Griffin, “Fundamental Study Of Fc-72 Pool Boiling Surface Temperature Fluctuations And Bubble Behavior,” no. 2008, pp. 2004–2019, 2008.

[18] R. Cole, “Bubble frequencies and departure volumes at subatmospheric pressures,” *AIChE J.*, vol. 13, no. 4, pp. 779–783, 1967.

[19] H. J. Ivey, “Relationships between bubble frequency, departure diameter and rise velocity in nucleate boiling,” *Int. J. Heat Mass Transf.*, vol. 10, no. 8, pp. 1023–1040, 1967.

[20] G. Tryggvason and A. Esmaeeli, “Computations of boiling flows,” *Proc. ASME Heat Transf. Eng. Summer Conf. 2004, HT/FED 2004*, vol. 3, no. 3, pp. 561–566, 2004.

[21] J. Buongiorno, L. W. Hu, G. Apostolakis, R. Hannink, T. Lucas, and A. Chupin, "A feasibility assessment of the use of nanofluids to enhance the in-vessel retention capability in light-water reactors," *Nucl. Eng. Des.*, vol. 239, no. 5, pp. 941–948, 2009.

[22] S. M. Kwark, M. Amaya, R. Kumar, G. Moreno, and S. M. You, "Effects of pressure, orientation, and heater size on pool boiling of water with nanocoated heaters," *Int. J. Heat Mass Transf.*, vol. 53, no. 23–24, pp. 5199–5208, 2010.

[23] H. Sakashita and A. Ono, "Boiling behaviors and critical heat flux on a horizontal plate in saturated pool boiling of water at high pressures," *Int. J. Heat Mass Transf.*, vol. 52, no. 3–4, pp. 744–750, 2009.

[24] Y. Takata, S. Hidaka, M. Masuda, and T. Ito, "Pool boiling on a superhydrophilic surface," *Int. J. Energy Res.*, vol. 27, no. 2, pp. 111–119, 2003.

[25] J. P. McHale and S. V. Garimella, "Bubble nucleation characteristics in pool boiling of a wetting liquid on smooth and rough surfaces," *Int. J. Multiph. Flow*, vol. 36, no. 4, pp. 249–260, 2010.

[26] S. Launay, A. G. Fedorov, Y. Joshi, A. Cao, and P. M. Ajayan, "Hybrid micro-nano structured thermal interfaces for pool boiling heat transfer enhancement," *Microelectronics J.*, vol. 37, no. 11, pp. 1158–1164, 2006.

[27] R. I. Vachon, G. E. Tanger, D. L. Davis, and G. H. Nix, "Pool boiling on polished and chemically etched stainless-steel surfaces," *J. Heat Transfer*, vol. 90, no. 2, pp. 231–238, 1968.

[28] D. Correlation, "Vachon1968 (1)," pp. 239–246, 2013.

[29] E. Demir, T. Izci, A. S. Alagoz, T. Karabacak, and A. Koşar, "Effect of silicon nanorod length on horizontal nanostructured plates in pool boiling heat transfer with water," *Int. J.*

Therm. Sci., vol. 82, no. 1, pp. 111–121, 2014.

[30] Y. H. Kim, K. J. Lee, and D. Han, "Pool boiling enhancement with surface treatments," *Heat Mass Transf. und Stoffuebertragung*, vol. 45, no. 1, pp. 55–60, 2008.

[31] M. Dadjoo, N. Etesami, and M. N. Esfahany, "Influence of orientation and roughness of heater surface on critical heat flux and pool boiling heat transfer coefficient of nanofluid," *Appl. Therm. Eng.*, vol. 124, pp. 353–361, 2017.

[32] A. Ustinov, V. Ustinov, and J. Mitrovic, "Pool boiling heat transfer of tandem tubes provided with the novel microstructures," *Int. J. Heat Fluid Flow*, vol. 32, no. 4, pp. 777–784, 2011.

[33] K. Pratik, A. Nammari, T. S. Ashton, and A. L. Moore, "Saturated pool boiling heat transfer from vertically oriented silicon surfaces modified with foam-like hexagonal boron nitride nanomaterials," *Int. J. Heat Mass Transf.*, vol. 95, pp. 964–971, 2016.

[34] S. H. Kim, G. C. Lee, J. Y. Kang, K. Moriyama, M. H. Kim, and H. S. Park, "Boiling heat transfer and critical heat flux evaluation of the pool boiling on micro structured surface," *Int. J. Heat Mass Transf.*, vol. 91, pp. 1140–1147, 2015.

[35] L. Duan, B. Liu, B. Qi, Y. Zhang, and J. Wei, "Pool boiling heat transfer on silicon chips with non-uniform micro-pillars," *Int. J. Heat Mass Transf.*, vol. 151, 2020.

[36] X. Ma and P. Cheng, "Dry spot dynamics and wet area fractions in pool boiling on micro-pillar and micro-cavity hydrophilic heaters: A 3D lattice Boltzmann phase-change study," *Int. J. Heat Mass Transf.*, vol. 141, pp. 407–418, 2019.

[37] D. Cooke and S. G. Kandlikar, "Pool boiling heat transfer and bubble dynamics over plain and enhanced microchannels," *J. Heat Transfer*, vol. 133, no. 5, 2011.

[38] A. Jaikumar and S. G. Kandlikar, "Enhanced pool boiling heat transfer mechanisms for

selectively sintered open microchannels," *Int. J. Heat Mass Transf.*, vol. 88, pp. 652–661, 2015.

[39] C. M. Patil and S. G. Kandlikar, "Pool boiling enhancement through microporous coatings selectively electrodeposited on fin tops of open microchannels," *Int. J. Heat Mass Transf.*, vol. 79, pp. 816–828, 2014.

[40] S. Vemuri and K. J. Kim, "Pool boiling of saturated FC-72 on nano-porous surface," *Int. Commun. Heat Mass Transf.*, vol. 32, no. 1–2, pp. 27–31, 2005.

[41] C. Young Lee, M. M. Hossain Bhuiya, and K. J. Kim, "Pool boiling heat transfer with nano-porous surface," *Int. J. Heat Mass Transf.*, vol. 53, no. 19–20, pp. 4274–4279, 2010.

[42] Y. Tang, B. Tang, Q. Li, J. Qing, L. Lu, and K. Chen, "Pool-boiling enhancement by novel metallic nanoporous surface," *Exp. Therm. Fluid Sci.*, vol. 44, pp. 194–198, 2013.

[43] K. H. Chu, Y. S. Joung, R. Enright, C. R. Buie, and E. N. Wang, "Hierarchically structured surfaces for boiling critical heat flux enhancement," *Appl. Phys. Lett.*, vol. 102, no. 15, 2013.

[44] H. W. Moon, Y. J. Yoon, J. H. Park, B. S. Myung, and D. E. Kim, "Dynamic wetting and boiling characteristics on micro-structured and micro/nano hierarchically structured surfaces," *Exp. Therm. Fluid Sci.*, vol. 74, pp. 19–26, 2016.

[45] B. Liu, J. Liu, Y. Zhang, J. Wei, and W. Wang, "Experimental and theoretical study of pool boiling heat transfer and its CHF mechanism on femtosecond laser processed surfaces," *Int. J. Heat Mass Transf.*, vol. 132, pp. 259–270, 2019.

[46] M. McCarthy, K. Gerasopoulos, S. C. Maroo, and A. J. Hart, "Materials, fabrication, and manufacturing of Micro/Nanostructured surfaces for phase-change heat transfer enhancement," *Nanoscale Microscale Thermophys. Eng.*, vol. 18, no. 3, pp. 288–310, 2014.

[47] D. E. Kim, D. I. Yu, D. W. Jerng, M. H. Kim, and H. S. Ahn, "Review of boiling heat transfer enhancement on micro/nanostructured surfaces," *Exp. Therm. Fluid Sci.*, vol. 66, pp. 173–196, 2015.

[48] D. Attinger *et al.*, "Surface engineering for phase change heat transfer: A review," *MRS Energy Sustain.*, vol. 1, pp. 1–40, 2014.

[49] M. M. Rahman and M. McCarthy, "Effect of Length Scales on the Boiling Enhancement of Structured Copper Surfaces," *J. Heat Transfer*, vol. 139, no. 11, pp. 1–9, 2017.

[50] M. Tetreault-Friend *et al.*, "Critical heat flux maxima resulting from the controlled morphology of nanoporous hydrophilic surface layers," *Appl. Phys. Lett.*, vol. 108, no. 24, 2016.

[51] H. Honda, H. Takamatsu, and J. J. Wei, "Enhanced boiling of FC-72 on silicon chips with micro-pin-fins and submicron-scale roughness," *J. Heat Transfer*, vol. 124, no. 2, pp. 383–390, 2002.

[52] B. Bon, J. F. Klausner, and E. Mckenna, "The Hoodoo: A New Surface Structure for Enhanced Boiling Heat Transfer," *J. Therm. Sci. Eng. Appl.*, vol. 5, no. 1, pp. 1–11, 2013.

[53] M. C. Lu, R. Chen, V. Srinivasan, V. P. Carey, and A. Majumdar, "Critical heat flux of pool boiling on Si nanowire array-coated surfaces," *Int. J. Heat Mass Transf.*, vol. 54, no. 25–26, pp. 5359–5367, 2011.

[54] Z. Yao, Y. W. Lu, and S. G. Kandlikar, "Effects of nanowire height on pool boiling performance of water on silicon chips," *Int. J. Therm. Sci.*, vol. 50, no. 11, pp. 2084–2090, 2011.

[55] A. Zou and S. C. Maroo, "Critical height of micro/nano structures for pool boiling heat transfer enhancement," *Appl. Phys. Lett.*, vol. 103, no. 22, 2013.

[56] A. Zou, D. P. Singh, and S. C. Maroo, “Early Evaporation of Microlayer for Boiling Heat Transfer Enhancement,” *Langmuir*, vol. 32, no. 42, pp. 10808–10814, 2016.

[57] M. M. Rahman, E. Ölçeroglu, and M. McCarthy, “Role of wickability on the critical heat flux of structured superhydrophilic surfaces,” *Langmuir*, vol. 30, no. 37, pp. 11225–11234, 2014.

[58] H. S. Ahn, C. Lee, J. Kim, and M. H. Kim, “The effect of capillary wicking action of micro/nano structures on pool boiling critical heat flux,” *Int. J. Heat Mass Transf.*, vol. 55, no. 1–3, pp. 89–92, 2012.

[59] H. S. Ahn *et al.*, “Pool boiling CHF enhancement by micro/nanoscale modification of zircaloy-4 surface,” *Nucl. Eng. Des.*, vol. 240, no. 10, pp. 3350–3360, 2010.

[60] S. Kumar C. S., Y. W. Chang, and P. H. Chen, “Pool-boiling heat-transfer enhancement on cylindrical surfaces with hybrid wettable patterns,” *J. Vis. Exp.*, vol. 2017, no. 122, 2017.

[61] C. S. Sujith Kumar, Y. W. Chang, and P. H. Chen, “Effect of heterogeneous wettable structures on pool boiling performance of cylindrical copper surfaces,” *Appl. Therm. Eng.*, vol. 127, pp. 1184–1193, 2017.

[62] S. G. Kandlikar, “A theoretical model to predict pool boiling CHF incorporating effects of contact angle and orientation,” *J. Heat Transfer*, vol. 123, no. 6, pp. 1071–1079, 2001.

[63] M. M. Rahman, E. Ölçeroɨlu, and M. McCarthy, “Scalable Nanomanufacturing of Virus-templated Coatings for Enhanced Boiling,” *Adv. Mater. Interfaces*, vol. 1, no. 2, pp. 1–6, 2014.

[64] J. S. Mehta and S. G. Kandlikar, “Pool boiling heat transfer enhancement over cylindrical tubes with water at atmospheric pressure, Part I: Experimental results for circumferential rectangular open microchannels,” *Int. J. Heat Mass Transf.*, vol. 64, pp. 1205–1215, 2013.

[65] L. H. Chien and R. L. Webb, “Visualization of pool boiling on enhanced surfaces,” *Exp. Therm. Fluid Sci.*, vol. 16, no. 4, pp. 332–341, 1998.

[66] G. Ribatski and J. M. S. Jabardo, “Experimental study of nucleate boiling of halocarbon refrigerants on cylindrical surfaces,” *Int. J. Heat Mass Transf.*, vol. 46, no. 23, pp. 4439–4451, 2003.

[67] S. B. Memory, D. C. Sugiyama, and P. J. Marto, “Nucleate pool boiling of R-114 and R-114-oil mixtures from smooth and enhanced surfaces-I. Single tubes,” *Int. J. Heat Mass Transf.*, vol. 38, no. 8, pp. 1347–1361, 1995.

[68] P. Hübner and W. Künstler, “Pool boiling heat transfer at finned tubes: Influence of surface roughness and shape of the fins,” *Int. J. Refrig.*, vol. 20, no. 8, pp. 575–582, 1997.

[69] D. Jung, K. An, and J. Park, “Nucleate boiling heat transfer coefficients of HCFC22, HFC134a, HFC125 and HFC32 on various enhanced tubes,” *Int. J. Refrig.*, vol. 27, no. 2, pp. 202–206, 2004.

[70] L. H. Chien and R. L. Webb, “A parametric study of nucleate boiling on structured surfaces part II: Effect of pore diameter and pore pitch,” *Am. Soc. Mech. Eng. Heat Transf. Div. HTD*, vol. 326, no. November 1998, pp. 137–143, 1996.

[71] Y. Chen, M. Groll, R. Mertz, and R. Kulenovic, “Bubble dynamics of boiling of propane and iso-butane on smooth and enhanced tubes,” *Exp. Therm. Fluid Sci.*, vol. 28, no. 2–3, pp. 171–178, 2004.

[72] D. Jung, H. Lee, D. Bae, and J. Ha, “Nucleate boiling heat transfer coefficients of flammable refrigerants on various enhanced tubes,” *Int. J. Refrig.*, vol. 28, no. 3, pp. 451–455, 2005.

[73] M. H. Saidi, M. Ohadi, and M. Souhar, “Enhanced pool boiling of R-123 refrigerant on two selected tubes,” *Appl. Therm. Eng.*, vol. 19, no. 8, pp. 885–895, 1999.

[74] S. Kotthoff, D. Gorenflo, E. Danger, and A. Luke, “Heat transfer and bubble formation in pool boiling: Effect of basic surface modifications for heat transfer enhancement,” *Int. J. Therm. Sci.*, vol. 45, no. 3, pp. 217–236, 2006.

[75] D. Gorenflo, E. Baumhögger, T. Windmann, and G. Herres, “Nucleate pool boiling, film boiling and single-phase free convection at pressures up to the critical state. Part I: Integral heat transfer for horizontal copper cylinders,” *Int. J. Refrig.*, vol. 33, no. 7, pp. 1229–1250, 2010.

[76] J. T. Cieiliński, “Nucleate pool boiling on porous metallic coatings,” *Exp. Therm. Fluid Sci.*, vol. 25, no. 7, pp. 557–564, 2002.

[77] J. H. Kim, K. N. Rainey, S. M. You, and J. Y. Pak, “Mechanism of nucleate boiling heat transfer enhancement from microporous surfaces in saturated FC-72,” *J. Heat Transfer*, vol. 124, no. 3, pp. 500–506, 2002.

[78] Omega, “Presure Trasnducer and Thermocouples type K,” *https://www.omega.com/en-us/sensors-and-sensing-equipment/pressure-and-strain/pressure-transducers/px01/p/PX01C1-300GV*.

[79] National Instrument, “PXI-6515,” *https://www.ni.com/es-mx/shop/hardware/products/pxi-digital-io-module.html?modelId=123285*.

Vita

Omar Hernandez Rodriguez has the Master of Science in Physics at University of Texas at El Paso, May 2018 – present. Thesis title: “Geant4 study of protons-body interactions” and Bachelor of Engineering in Physics in Universidad Autónoma de Ciudad Juárez, May 2015.

Graduate Teaching Assistant in Department of Physics at University of Texas at El Paso, August 2016 - 2018. Responsibilities include: assisting professors with the preparation and presentation of undergraduate courses, grading, and tutoring. And presentation of Geant4 study of protons-body interactions.in the meeting of the American Physical Society at University of Texas at Dallas, Dallas, Texas, October 2017. Actual member of American Physical Society.

Graduate Teaching Assistant in Department of Mechanical Engineering at University of Texas at El Paso, August 2018 - 2019. Responsibilities include: assisting professors with the preparation and presentation of undergraduate courses, grading, and tutoring.

Graduate Research Assistant in Department of Mechanical Engineering at University of Texas at El Paso, August 2019 - present. Responsibilities include: research assisting professors with the design of pool boiling and flow boiling facility.

Contact Information: ohernandez21@miners.utep.edu

This thesis was typed by Omar Hernandez Rodriguez